Structure-function Relationship of the β-hairpin Loop in the N-terminal Domain and the Zinc-binding Motif of Thermolysin

MENACH EVANS PKEMOI

2014

Contents

Abbreviations

CD	circular dichroism
DPP III	dipeptidyl peptidase III
FAGLA	*N*-[3-(2-furyl)acryloyl]-glycyl-L-leucine amide
Gly-D-Phe	glycyl-D-phenylalanine
HEPES	2-[4-(2-hydroxyethyl)-1-piperazinyl]ethanesulfonic acid
k_{cat}	molecular activity
k_{cat}/K_m	specificity constant
K_e	proton dissociation constant
K_m	Michaelis constant
k_{obs}	first-order rate constant for thermal inactivation
MES	2-(*N*-morpholino)ethanesulfonic acid
npr	neutral protease
OD	optical density
SDS-PAGE	sodium dodecyl sulfate polyacrylamide gel electrophoresis
TLN	thermolysin
Tris	tris(hydroxymethyl)aminomethane
TAPS	*N*-tris(hydroxymethyl)methyl-3-aminopropanesulfonic acid
UV	ultra violet
WT	wild-type thermolysin
ZDFM	*N*-carbobenzoxy-L-aspartyl-L-phenylalanine methyl ester

Introduction

Thermolysin (TLN) [EC 3.4.24.27] is a thermostable neutral metalloproteinase that belongs to the gluzincins family of clan MA, subclan MA(E). It was originally identified in the culture broth of *Bacillus thermoproteolyticus* (*1–3*). It contains one zinc ion that is essential for catalysis and four calcium ions for structural stability (*4–6*). It has a molecular mass of 34.6 kDa and comprises 316 amino acid residues whose sequence is known (*7–8*). The overall structure of TLN consists of two domains, a β-rich N-terminal domain (Ile1-Asp138) and an α-helical C-terminal domain (Asp150-Lys316) (*9–11*). The domains are connected by an α-helix (Val139-Thr149) located at the bottom of the active site cleft (*10*). The active site is composed of one zinc ion and five polypeptide regions: N-terminal sheet (Asn112-Trp115), α-helix 1 (Val139-Thr149), C-terminal loop 1 (Asp150-Gly162), α-helix 2 (Ala163-Val176), and C-terminal loop 2 (Gln225-Ser234) (*12*).

The α-helix 1 located at the bottom of the active site contains the zinc-binding motif sequence His-Glu-x-x-His (HEXXH). This motif sequence is highly conserved in zinc-dependent metalloproteases (zincins), a broad group of proteins involved in many metabolic and regulatory functions, and found in virtually all forms of life (*13*). Some other mono-zinc proteases have different zinc-binding motifs, for example HEXXXH in dipeptidyl peptidase III (DPP III) (*14*). Almost all Co(II)- or Mn(II)-substituted enzymes maintain the catalytic activity of their zinc counterparts. Based on structural studies of various metal-substituted enzymes, the metal coordination geometries of both active and inactive Cu(II)-substituted enzymes have been shown to be the same as those of the wild-type Zn(II) enzymes (*15*). This implies that the enzymatic activity of a metal-ion-substituted zinc metalloprotease may depend on the flexibility of the catalytic domain.

TLN catalyzes primarily the hydrolysis of peptide bonds containing hydrophobic amino acid residues (*16, 17*). In addition, it catalyzes peptide bond formation through reverse reaction of hydrolysis, a property which has been exploited industrially. The

most extensive use is in the synthesis of *N*-carbobenzoxy-L-aspartyl-L-phenylalanine methyl ester (ZDFM) from *N*-carbobenzoxy-L-aspartic acid (ZD) and L-phenylalanine methyl ester (FM) (*18, 19*). ZDFM is a precursor of an artificial sweetener, aspartame, which is 200 times sweeter than sucrose. Because of its economic importance the improvement of its activity and stability are important subjects.

TLN activity increases in an exponential fashion with increasing concentrations of neutral salts (1–5 M) (*17*, *18, 20–23*). The ratios of the specificity constant, k_{cat}/K_m, at 4.0 M NaCl to that at 0 M NaCl of WT is 13–15 in the hydrolysis of the neutral substrate *N*-[3-(2-furyl)acryloyl]-glycyl-L-leucine amide (FAGLA) and 6–7 in the hydrolysis of the negatively charged substrate ZDFM at pH 7.0 at 25°C (*19–22*). The degree of activation at x molar NaCl in the hydrolysis of FAGLA at pH 7.5 takes the form 1.9^x. Activation is solely due to an increase in k_{cat}; the K_m is unaffected during activation. Activation is highest in the presence of NaCl or NaBr. This has been related to specific interactions between cations and TLN, and the magnitude of activation is in the order $Na^+ > K^+ > Li^+$. Though the exact mechanism of activation has not been clearly elucidated, the activation order suggests the degrees of hydration coupled with specific electrostatic interactions with TLN residues are involved in the activation mechanism. Interestingly, virtually all highly active TLN variants produced by site-directed mutagenesis generally exhibited drastically diminished degree of NaCl-induced activation.

TLN's stability increases in the range 0–2 M NaCl (*17*). The ratio of the first-order rate constant for thermal inactivation (k_{obs}) at 70ºC at 0 M NaCl to that at 1 M NaCl of TLN is about 3 (*17*) This stabilizing effect decreases above 2 M NaCl (*17*). The activation energy, E_a, for thermal inactivation is 15 kcal/mol at 0 M NaCl, and increases up to 30–33 kcal/mol on the addition of 0.5–1.5 M NaCl. Further increases in sodium chloride concentration decrease the E_a value, and at 4.0 M NaCl E_a is almost the same as that at 0 M NaCl. The stability dependence on NaCl concentration is different from that of activity, suggesting that the effects of NaCl on activity and stability are independent. TLN has been demonstrated to be not only a thermophilic enzyme but also a highly halophilic one.

The general objective of this study was to examine the structure-function relationship of the β-hairpin loop in the N-terminal domain and the zinc-binding motif of TLN. Specifically, the desire was to generate TLN variants with (i) altered substrate specificity, (ii) enhanced activity and/or stability, (iii) altered catalytic metal-ion preference, and (iv) to explore the relation between activity enhancements induced by NaCl versus that caused by mutation, especially where the activity-enhancing mutation simultaneously affects NaCl-induced activation. In Chapters 1 and 2, the roles of Asn116 and Gly117 in the β-hairpin loop of the Asn112-Trp115 and Ser118-Tyr115 strands of the active site of TLN are examined. Chapter 3 explores the mechanism of salt-induced activation and stabilization of TLN by comparing the effects of Asn116→Asp and Asp150→Glu mutations on NaCl-induced activation and stabilization. Chapter 4 examines the effects of conversion of the zinc-binding motif sequence of TLN from HEXXH to HEXXXH on catalytic activity and stability. Throughout this study, the mutation of a residue e.g. Asn116 to Asp was designated as Asn116→Asp, and the TLN variant bearing the mutation was designated as N116D.

Chapter 1

Effects of Site-directed Mutagenesis of the Loop Residue of the N-terminal Domain Gly117 of Thermolysin on Its Catalytic Activity

Introduction

The active site of TLN is composed of one zinc ion and five polypeptide regions (*12*). Site-directed mutagenesis studies of TLN have been done extensively in the five regions, especially on its active-site residues (*24–32*). Of the active-site residue variants, L144S, D150E, and I168A exhibited higher activities than WT in the hydrolysis of FAGLA, a widely used substrate for TLN (*18, 33*). L155A had higher stability than WT (*27, 28*). N112D (*28*), F114H (*10*), and Q225A (*29*) had modified pH-activity profiles.

In the N-terminal domain of TLN, two parallel polypeptide strands, Asn112-Ala113-Phe114-Trp115 and Ser118-Gln119-Met120-Val121-Tyr122, are connected by a short loop, Asn116-Gly117, to form an anti-parallel β-sheet at the active site (Fig. 1). The Asn112-Trp115 strand is located in the active site, while the Ser118-Tyr122 strand and the Asn116-Gly117 loop are located outside the active site. The objective of this study was to explore the catalytic role of Gly117 by site-directed mutagenesis. TLN variants were expressed in *Escherichia coli*, purified, and characterized for their activities and thermal stabilities in the hydrolysis of FAGLA and ZDFM.

Materials and Methods

Materials – Bovine milk casein of Hammerstein grade (lot WKL1761) was purchased from Wako Pure Chemical (Osaka, Japan). FAGLA (lot 111K1764) was

purchased from Sigma (St. Louis, MO). The concentrations of FAGLA and ZDFM were determined spectrophotometrically using the molar absorption coefficients, ε_{345} = 766 M^{-1} cm^{-1} and ε_{257} = 387 M^{-1} cm^{-1}, respectively (*18, 22*).

Bacterial strains, plasmids, and transformation – E. coli K12 JM109, *recA1, endA1, gyrA96, thi, hsdR17, supE44, relA1,* Δ(*lac-proAB*), *F'*(*traD36, proAB*$^{+}$ *lac*^{Iq}, *lacZ*Δ*M15*), was used. pTMP1 is an expression plasmid that co-expresses the mature sequence of TLN that contains the pelB leader sequence at its N-terminus and the pre-prosequence (*34*). Site-directed mutagenesis was carried out using a Quikchange™ site-directed mutagenesis kit (Stratagene, La Jolla, CA). The nucleotide sequences of the mutated TLN genes were verified with a Shimadzu DNA sequencer DSQ-2000 (Shimadzu, Kyoto, Japan). JM109 cells were transformed with the resulting plasmids and cultured in L broth. Ampicillin was used at a concentration of 50 μg/ml.

Purification of TLN variants – TLN variants were expressed into the supernatant of *E. coli* cultures and purified to homogeneity by sequential column chromatography of the supernatant (*34–36*). Briefly, for seed culture, 5 ml of L broth in a 20-ml test tube was inoculated with glycerol stock of transformed JM109 cells and grown with shaking at 37ºC for 12 h. The culture (5 ml) was supplemented with 500 ml of L broth in a 1-liter flask and incubated at 37ºC for 48 h, with 0.1% (w/v) anti-foam A (Sigma) and vigorous aeration with an air pump. The supernatant was applied to a column packed with Toyopearl Phenyl-650M gel (Tosoh, Tokyo). Active fractions were pooled and then applied to a column of Gly-D-Phe coupled to CNB-activated Sepharose 4B resin (Amersham-Pharmacia Biotech, Uppsala, Sweden). Prior to kinetic measurement, the preparations were desalted using pre-packed PD-10 gel filtration columns (Amersham Biosciences, Uppsala, Sweden).

SDS-PAGE – SDS-PAGE was performed in a 12.5% polyacrylamide gel under reducing conditions by the method of Laemmli (*37*). A constant current of 40 mA was applied for 40 min. Supernatants were reduced by treatment with 2.5%

2-mercaptoethanol at 100ºC for 10 min. Proteins were stained with Coomassie Brilliant Blue R-250. A molecular-mass marker kit consisting of rabbit muscle phosphorylase *b* (97.4 kDa), bovine serum albumin (66.3 kDa), rabbit muscle aldolase (42.4 kDa), bovine erythrocyte carbonic anhydrase (30.0 kDa), soybean trypsin inhibitor (20.1 kDa), and hen egg white lysozyme (14.4 kDa) was from Daiichi Pure Chemicals (Tokyo).

Two-dimensional gel electrophoresis – Isoelectric focusing (IEF) was done with agarGel (Atto, Tokyo), containing carrier ampholytes (pH 3–10) and discRun (Atto). A constant voltage of 300 V was applied for 210 min. Purified WT or G117E (50 µl of 2 µg/ml in 60 mM Tris-HCl pH 8.9, 5 M urea, 1 M thiourea, 1% (v/v) 3-[(3-cholamidopropyl)dimethylammonio]-1-propane sulfonate (CHAPS), 1% (v/v) Triton X-100, and 1% (w/v) DTT) were applied to agarGel. After IEF, the gels were expelled from the tubes and equilibrated in 2.5% (w/v) trichloroacetic acid for 3 min, followed by immersion in water. They were then placed on top of a 12.5% polyacrylamide gel, and SDS-PAGE was done as described above.

Hydrolysis of casein – Casein-hydrolyzing activity was measured by methods described previously (*3, 31*). The TLN solution (0.5 ml) was added to 1.5 ml of a solution containing 1.33% (w/v) casein and 40 mM Tris-HCl pH 7.5, and incubated at 25ºC for 30 min. The reaction was stopped by the addition of 2 ml of a solution containing 0.11 M trichloroacetic acid, 0.22 M sodium acetate, and 0.33 M acetic acid. After 1 h of incubation at 25ºC, the reaction mixture was filtered through Whatman no. 2 filter paper (diameter 70 mm), and the absorbance (A_{275}) at 275 nm was measured. One proteolytic unit (PU) is defined as the amount of enzyme activity that liberates a quantity of acid soluble peptides that corresponds to an increase in A_{275} of 0.0074 (A_{275} of 1 µg of tyrosine)/min.

Spectrophotometric analysis of the TLN-catalyzed hydrolysis of FAGLA – TLN-catalyzed hydrolysis of FAGLA was measured by the decrease in absorbance (A_{345}) at 345 nm (*17, 18*). The amount of FAGLA hydrolyzed was evaluated using the

molar absorption difference due to hydrolysis, $\Delta\varepsilon_{345}$ = -310 M^{-1} cm^{-1}, at 25ºC (*17, 18, 32*). The reaction was carried out in 40 mM acetate-NaOH buffer at pH 4.0–5.5, 40 mM MES-NaOH buffer at pH 5.5–7.0, 40 mM HEPES-NaOH buffer at pH 7.0–8.5, and TAPS-NaOH buffer at pH 8.0–9.0, each of which contained 10 mM $CaCl_2$, at 25ºC. Hydrolysis was carried out under pseudo first-order conditions, where the substrate concentration is much lower than the K_m (> 30 mM) (*18*) because of the sparing solubility (< 6 mM) of FAGLA (*16, 18, 32*). Under the conditions, the kinetic parameters, K_m and k_{cat}, cannot be determined separately, and enzyme activity was evaluated by the k_{cat}/K_m. The intrinsic k_{cat}/K_m, ($(k_{cat}/K_m)_o$), and the proton dissociation constants (K_{e1} and K_{e2}) for the bell-shaped pH-dependence of activity (k_{cat}/K_m) were calculated from eq. 1 by a non-linear least-squares regression method with Kaleida Graph Version 3.5 (Synergy Software, Essex, VT):

$$(k_{cat}/K_m)_{obs} = (k_{cat}/K_m)_o / \{1 + ([H] / K_{e1}) + (K_{e2} / [H])\} \quad (1)$$

In this equation, $(k_{cat}/K_m)_{obs}$ and [H] are the k_{cat}/K_m values observed and the proton concentration, respectively, at a specified pH, and K_{e1} and K_{e2} correspond to the pK_as in the acidic and alkaline sides of the pH-dependence curve of $(k_{cat}/K_m)_{obs}$.

Spectrophotometric analysis of the TLN-catalyzed hydrolysis of ZDFM – TLN-catalyzed hydrolysis of ZDFM was measured by following the decrease in absorbance (A_{224}) at 224 nm (*18*). The amount of ZDFM hydrolyzed was measured using the molar absorption difference due to hydrolysis, $\Delta\varepsilon_{224}$ = -493 M^{-1} cm^{-1}, at 25ºC (*17*). The reaction was carried out with TLN in 40 mM Tris-HCl buffer (pH 7.5) containing 10 mM $CaCl_2$ at 25ºC. The kinetic parameters, k_{cat} and K_m, were determined with Kaleida Graph Version 3.5, based on the Michaelis-Menten equation using the non-linear least-squares method (*38*).

Thermal inactivation of TLN – TLN (0.5–8 μM) in 40 mM HEPES-NaOH buffer pH 7.5 containing 10 mM $CaCl_2$ was incubated at 80ºC for 0–24 min. Then it was

incubated at 25ºC for 1 min. The remaining activity of TLN toward FAGLA hydrolysis was determined as described above. Under the assumption that thermal inactivation of TLN is irreversible and consists of only one step (*31, 32 ,39*), the k_{obs} was evaluated by plotting the logarithm of the residual activity (k_{cat}/K_m) against the duration of thermal treatment.

Results

Production of Gly117 variants to homogeneity – Gly117 was changed into one of the negatively charged amino acid residues (Asp and Glu), one of the positively charged ones (Lys and Arg), or an uncharged one (Ala). WT and variants were expressed in *E. coli* and purified from the supernatants.

Figure 2 shows a time course for the cultures of the transformants. In the transformants with the expression plasmids for WT and G117E, casein hydrolysis activities appeared in the supernatants and increased progressively even after OD_{600} reached maximum. In the transformants with the expression plasmid for G117D, G117K, and G117R, low casein hydrolysis activity appeared in the supernatants and increased slightly with time. In the transformants with the expression plasmid for G117A, casein hydrolysis activities did not appear in the supernatants.

On SDS-PAGE, under reducing conditions, of the culture supernatants of the *E. coli* cells transformed with the expression plasmids for WT and the Gly117 variants, the 34.6-kDa protein band was clearly detected for WT, G117E, and G117K, but was hardly detected for G117A, G117D, or G117R. Figure 3 shows SDS-PAGE of the purified WT and the Gly117 variants, except for G117A. The TLN thus obtained yielded a single band with a molecular mass of 34.6 kDa. From 380–850 ml of the culture supernatants, 1.1 mg of WT, 0.04 mg of G117D, 1.8 mg of G117E, 0.10 mg of G117K, and 0.10 mg of G117R were recovered. Purified G117A was not obtained. Isoelectric focusing showed that the p*I* values of WT and G117E were 5.3 and 4.8, respectively (data not shown), indicating that the pI value of TLN was shifted by 0.5 pH

unit by the mutation Gly117→Glu.

Characterization of Gly117 variants – The specific activities of WT, G117D, G117E, G117K, and G117R in the hydrolysis of casein were 11,000, 2,000, 12,000, 3,200, and 2,900 units/mg, respectively, indicating that the specific activity of G117E was almost the same as that of WT, while those of G117D, G117K, and G117R were 20–30% of that of WT. We did not attempt further characterization of G117D due to paucity of the purified enzyme.

Figure 4A shows the pH-dependence of the k_{cat}/K_m of the TLN-catalyzed hydrolysis of FAGLA at 25ºC. All the plots showed bell-shaped curves, with an optimal pH of about 7. The $(k_{cat}/K_m)_o$, pK_{e1}, and pK_{e2} values are summarized in Table 1. The $(k_{cat}/K_m)_o$ values for G117E, G117K, and G117R were 80, 40, and 40%, respectively, of that of WT. The pK_{e1} and pK_{e2} values of the variants were similar to those of WT, except for the pK_{e2} value for G117R (8.6 ± 0.1), which was higher by 0.4 ± 0.3 units than that for WT (8.2 ± 0.2).

Figure 4B shows the dependence of the initial reaction rate (v_o) of the TLN-catalyzed hydrolysis of ZDFM at pH 7.5 at 25ºC on substrate concentration. All the plots showed saturated profiles. The k_{cat} and K_m values are summarized in Table 2. The k_{cat}/K_m values of G117E, G117K, and G117R were 130, 80, and 50%, respectively, of that of WT. The high k_{cat}/K_m value of G117E was ascribed to its high k_{cat} value.

We have reported that TLN activity increases with increasing concentration of neutral salts such as NaCl, and that the degree of NaCl-induced activation, which is defined as the ratio of the k_{cat}/K_m value at 4.0 M NaCl to that at 0 M NaCl, is in the range of 13–15 (*22*). Table 3 shows the k_{cat}/K_m values at 0 and 4.0 M NaCl in the hydrolysis of FAGLA and the degrees of NaCl-induced activation. The degrees of activation of G117E, G117K, and G117R were 90, 30, and 50%, respectively, of that of WT.

Figure 5 shows the time-dependence of thermal inactivation of the TLN variants at 80ºC. Inactivation followed pseudo first-order kinetics. The k_{obs} values are summarized in Table 4. The order for k_{obs} was G117K > G117R > G117E > WT. Thus

thermal inactivation of TLN at 80ºC was enhanced in the variants in the order G117K > G117R > G117E.

Discussion

Altered substrate specificity of G117E – In TLN, the S1 subsite is constituted by Phe114, and the S1′ subsite by Phe130, Leu133, Val139, Ile188, Gly189, Val192, and Leu202 (*9, 10, 25, 29*). Crystallographic analysis of the complex of TLN and an analog of the tetrahedral intermediate carbobenzoxy-Gly^{P}-L-Leu-L-Leu ("Gly^{P}" indicates the tetrahedral phosphorus of a phosphonamidate moiety corresponding to the trigonal carbon of the peptide linkage) revealed the postulated hydrogen bonds between TLN and the substrate, ND2 of Asn112 and O of the P2′ residue, OD1 of Asn112 and N of the P2′ residue, O of Ala113 and N of P1′ Leu, and N of Trp115 and O of P2 residue (*40*). Based on these findings, we speculate as follows: (i) TLN variants with altered substrate specificity can be obtained if the geometry of the S1 and S1′ subsites is changed without much affecting the backbone structure of the Asn112-Trp115 strand, and (ii) the geometry of the Asn112-Trp115 strand can be changed by mutation of Gly117, because the Asn116-Gly117 loop connects the Asn112-Trp115 strand and the Ser118-Tyr122 strand, and Gly is the most flexible amino acid residue.

The specific activities of G117E and WT in the hydrolysis of casein were almost the same, described in "Results". However, the k_{cat}/K_m value in the hydrolysis of FAGLA of G117E was slightly lower than that of WT (Fig. 4A, Table 1), while the k_{cat}/K_m value in the hydrolysis of ZDFM of G117E was slightly higher than that of WT (Fig. 4B, Table 2). The enhanced k_{cat}/K_m value of G117E in the hydrolysis of ZDFM is ascribed to an increase in k_{cat}. FAGLA and ZDFM are substrates routinely used in the characterization of TLN (*3, 18*) and neutral proteases from *B. stearothermophilus* (*41–43*). FAGLA is a poorly soluble neutral dipeptide, while ZDFM is a negatively charged dipeptide. We have reported several TLN variants, L144S, D150E, and I168A, with higher FAGLA- and ZDFM-hydrolyzing activities than WT (*12, 31, 32*). In contrast,

G117E is the first TLN variant with lower FAGLA-hydrolyzing and higher ZDFM-hydrolyzing activities. Our strategy appears to have been effective in altering the substrate specificity of TLN.

Decreased production levels of G117A and G117D – G117A was not produced at detectable levels in the supernatant of the *E. coli* transformants (Figs. 2 and 3). For their expression, we used an *E. coli* expression system that does not require autocatalytic cleavage. In this system, the mature domain of TLN, containing an NH_2-terminal pectate lyase B leader sequence and the pre-prodomain of TLN, were co-expressed constitutively in *E. coli* as independent polypeptides under the original promoter sequences in the *npr* gene, which encodes TLN (*34*). Indeed, all 72 active-site TLN variants were produced at similar levels by this system whether or not they retained activity (*34*). Considering that Ala is more hydrophobic than Gly, the introduced Ala117 might be oriented into a polar environment or outside the protein core, rendering the protein unstable.

G117D was produced at detectable levels in the supernatant of the *E. coli* transformants, but was scarcely purified (Figs. 2 and 3). Asp and Glu have similar characteristics: the pK_{e1} of their side chains in proteins are 4.4–4.6, their hydrophobicity scores are -3.5; and their volumes are 125 and 155 $Å^3$, respectively (*44*). Currently there is no explanation as to why the mutation Gly117→Glu is favourable, while Gly117→Asp is not favourable.

Decreased activities and stabilities of G117K and G117R – In the hydrolysis of FAGLA and ZDFM, the k_{cat}/K_m values of G117K and G117R were 40–60% of those of WT (Tables 1 and 2), while the degrees of salt-induced activation were 30–50% of that of WT (Table 3), and the k_{obs} values for thermal inactivation at 80ºC were 220–400% of that of WT (Table 4). We speculate that the positive charge introduced at position 117 affects the geometry of the Asn112-Trp115 strand and decreases the activity and stability of TLN. In regard to this, according to the crystal structure of TLN (Protein Data Bank no. 8TLN), the distance OD2 of Asp150 and Cα of Gly117 is only 4.2 Å.

Asp150 is located at C-terminal loop 1 (Asp150-Gly162) in the active site. We have found that D150E showed higher activity, while D150H and D150W showed higher stability (*12*). We presume that introduced Lys or Arg at position 117 interacts with Asp150, rendering the protein less active and stable.

TLN is a representative zinc metalloproteinase with high activity and stability. However, if its substrate specificity can be altered as we hope, it might provide many benefits to industry. Recent crystallographic analyses of aminopeptidase N have revealed that aminopeptidase N and TLN are strikingly similar in the structure of the C-terminal, but not so in the N-terminal domain (*46, 47*). There is a possibility that aminopeptidase activity can be generated in TLN by introducing negative charges that can recognize the positive charges of the N-terminal amino nitrogen of the substrate. In conclusion, Gly117 plays an important role in the activity and stability of TLN, presumably by affecting the geometry of the Asn112-Trp115 and Ser118-Tyr122 strands.

Table 1. pK_e and intrinsic k_{cat}/K_m ($(k_{cat}/K_m)_o$) values of WT and its variants in the hydrolysis of FAGLA at 25°C.

TLN	pK_{e1}	pK_{e2}	$(k_{cat}/K_m)_o$ (mM^{-1} s^{-1})
WT	5.1 ± 0.2 (0.0)	8.2 ± 0.2 (0.0)	40 ± 3 (1.0)
G117E	5.1 ± 0.2 (0.0)	8.3 ± 0.1 (+0.1)	33 ± 2 (0.8)
G117K	5.1 ± 0.1 (0.0)	8.3 ± 0.1 (+0.1)	16 ± 3 (0.4)
G117R	5.2 ± 0.1 (+0.1)	8.6 ± 0.1 (+0.4)	15 ± 2 (0.4)

Average of triplicate determinations with SD values are shown. Numbers in parentheses indicate ΔpK_e as compared to those of WT and the $(k_{cat}/K_m)_o$ relative to that of WT.

Table 2. Kinetic parameters of the WT and its variants in the hydrolysis of ZDFM at 25ºC.

TLN	K_m (mM)	k_{cat} (s^{-1})	k_{cat}/K_m (mM^{-1} s^{-1})
WT	0.42 ± 0.04 (1.0)	7.9 ± 0.3 (1.0)	18.8 ± 1.9 (1.0)
G117E	0.44 ± 0.03 (1.0)	10.5 ± 0.3 (1.3)	23.9 ± 2.4 (1.3)
G117K	0.57 ± 0.05 (1.4)	8.4 ± 0.3 (1.1)	14.7 ± 1.4 (0.8)
G117R	0.50 ± 0.04 (1.2)	4.8 ± 0.2 (0.6)	9.6 ± 0.9 (0.5)

Average of triplicate determinations with SD values are shown. Numbers in parentheses indicate values relative to those of WT.

Table 3. Degree of salt-induced activation of WT and its variants in the hydrolysis of FAGLA at 25ºC.

TLN	k_{cat}/K_m (mM^{-1} s^{-1})		B/A
	0 M NaCl (A)	4 M NaCl (B)	
WT	40 ± 3 (1.0)	600 ± 20 (1.0)	15 (1.0)
G117E	33 ± 2 (0.8)	476 ± 16 (0.8)	14 (0.9)
G117K	16 ± 3 (0.4)	60 ± 2 (0.1)	4 (0.3)
G117R	15 ± 2 (0.4)	105 ± 1 (0.2)	7 (0.5)

The reaction was carried out in 40 mM HEPES-NaOH buffer at pH 7.5, containing 10 mM $CaCl_2$, at 25ºC. Average of triplicate determinations with the SD value is shown. Numbers in parentheses indicate values relative to those of WT.

Table 4. Thermal stability of WT and its variants.

TLN	k_{obs}[a] x 10^4 (s^{-1})
WT	6.3 ± 0.4 (1.0)
G117E	9.6 ± 0.5 (1.5)
G117K	25 ± 2 (4.0)
G117R	14 ± 2 (2.2)

[a]k_{obs} determined at 80ºC. The average of triplicate determinations with the SD value is shown. Numbers in parentheses indicate values relative to that of WT.

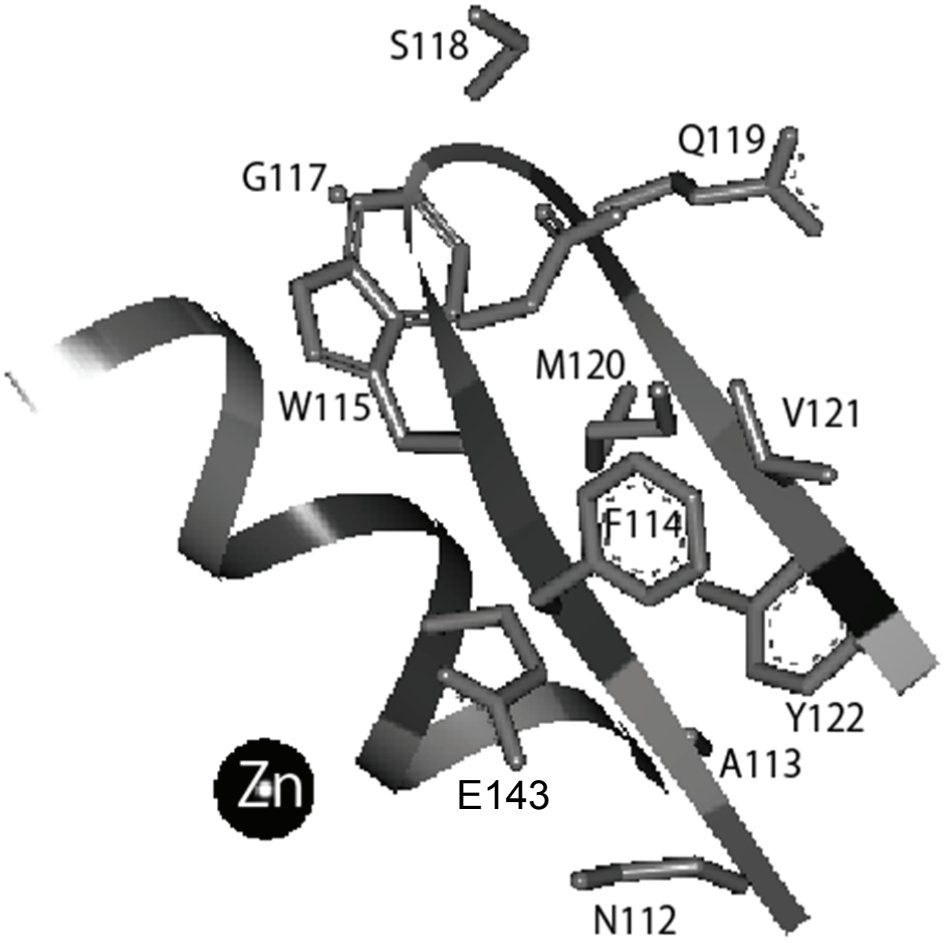

Fig. 1. Close-up view of the active site of TLN. The structure is based on Protein Data Bank no. 8TLN. The main chain is shown as a ribbon model. Side chains of the residues of the Asn112-Ala113-Phe114-Trp115 strand, the Asn116-Gly117 loop, the Ser118-Gln119-Met120-Val121-Tyr122 strand, and the catalytically important residue Glu143 are shown as ball and stick.

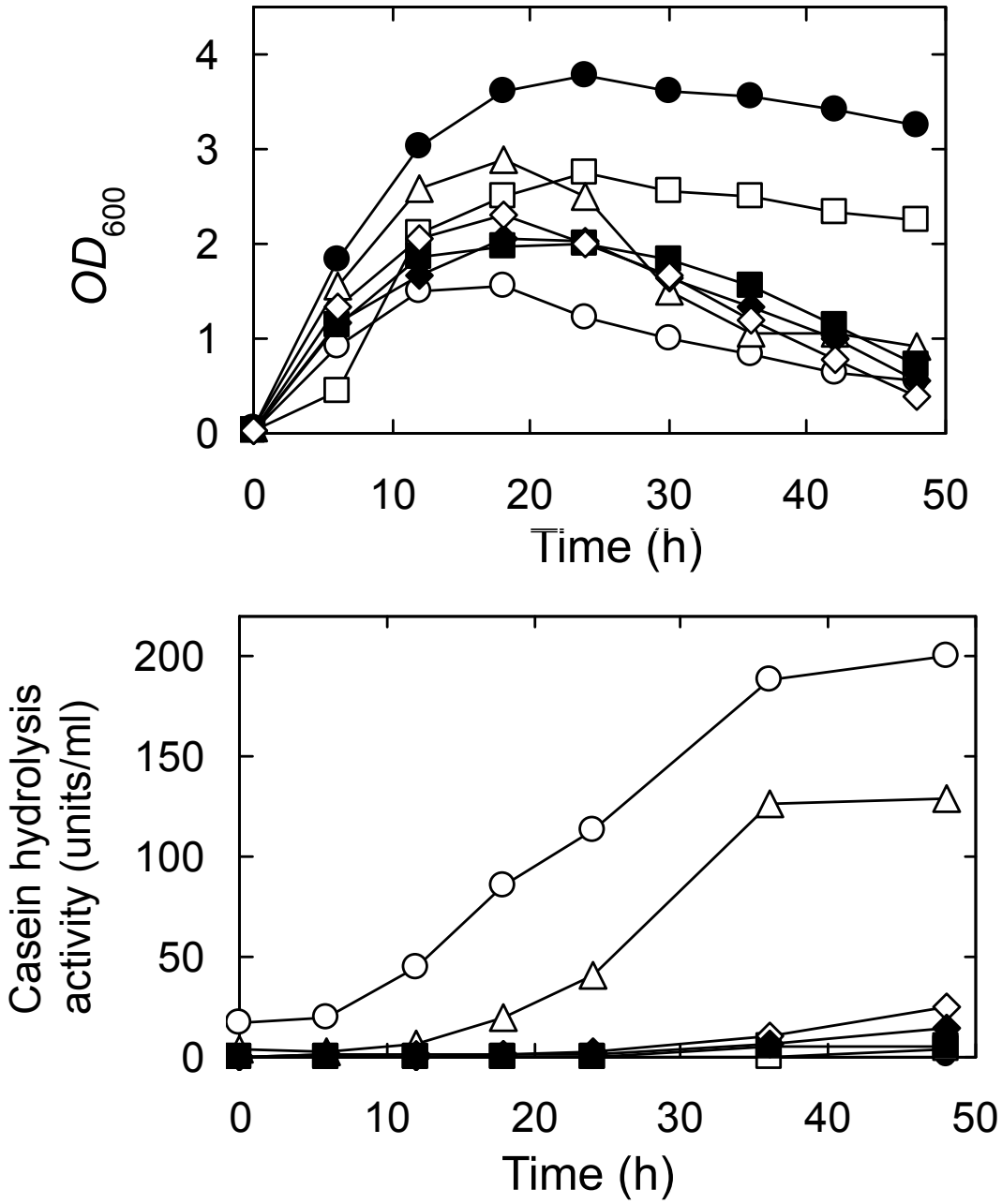

Fig. 2. Culturing of *E. coli*. (A) Cell densities (OD_{600}) of the culture. (B) Casein hydrolysis activity of the supernatants. JM109 cells transformed with pUC19 (●) and expression plasmids for the WT (○), G117A (□), G117D (■), G117E (△), G117K (◇), and G117R (◆) are cultured. Zero hour means start of test tube-shake culture.

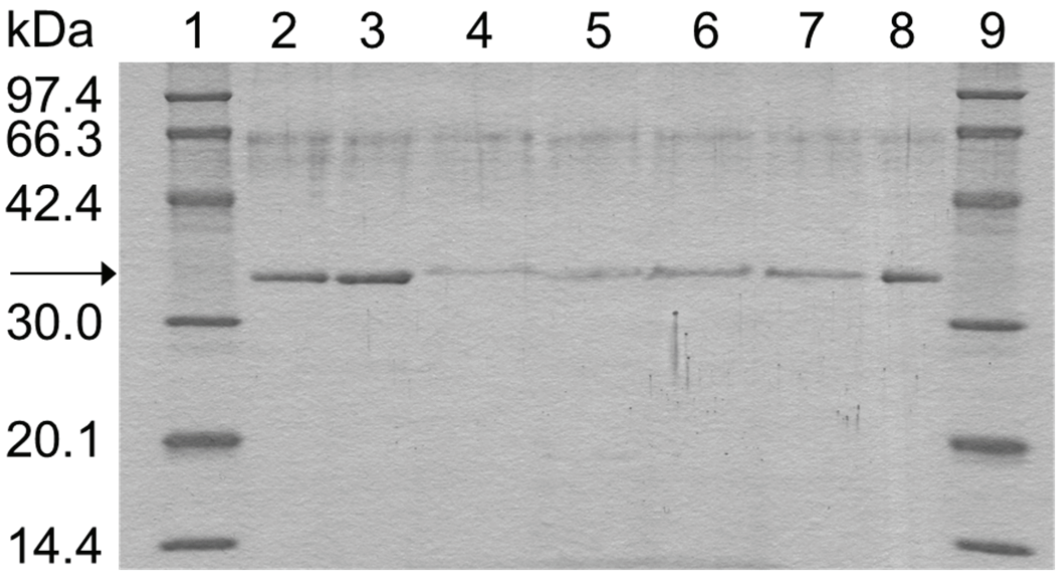

Fig. 3. Coomassie Brilliant Blue-Stained 12.5% SDS-PAGE gel. Marker proteins (lanes 1 and 9), native TLN purified from *B. thermoproteolyticus* (lanes 2 and 8), WT (lane 3), G117D (lane 4), G117E (lane 5), G117K (lane 6), and G117R (lane 7). The arrow indicates the band corresponding to mature TLN.

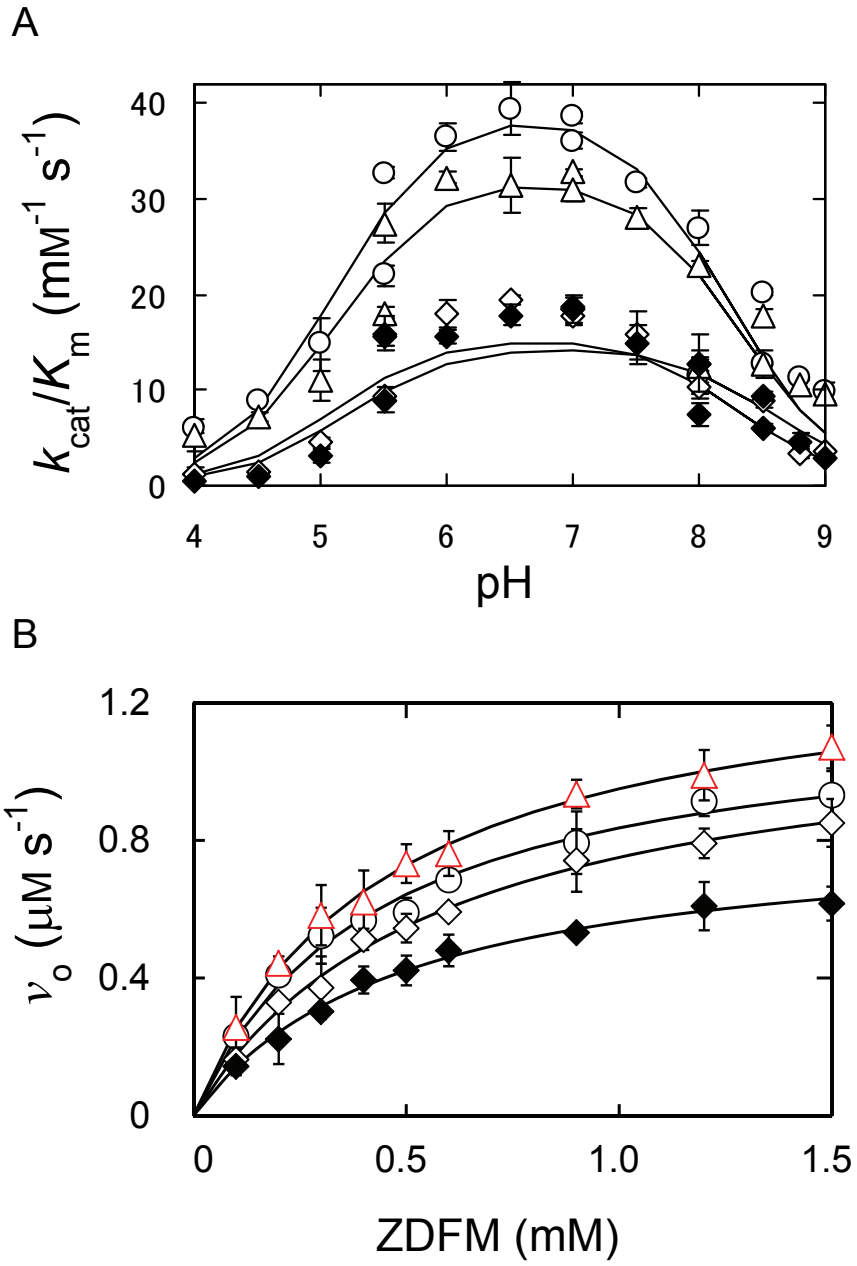

Fig. 4. Characterization of TLN variants. (A) Effect of pH on the initial reaction rate (v_o) in the TLN-catalyzed hydrolysis of FAGLA. The reaction was carried out with initial concentrations of enzyme and FAGLA of 100 nM and 400 μM respectively at 25ºC. (B) Dependence on the substrate concentration of v_o in the TLN-catalyzed hydrolysis of ZDFM. The reaction was carried out with an initial enzyme concentration $[E]_o$ of 100 nM at 25ºC. Symbols: WT (○), G117E (△), G117K (◇), and G117R (◆). Error bars indicate SD values for triplicate measurements.

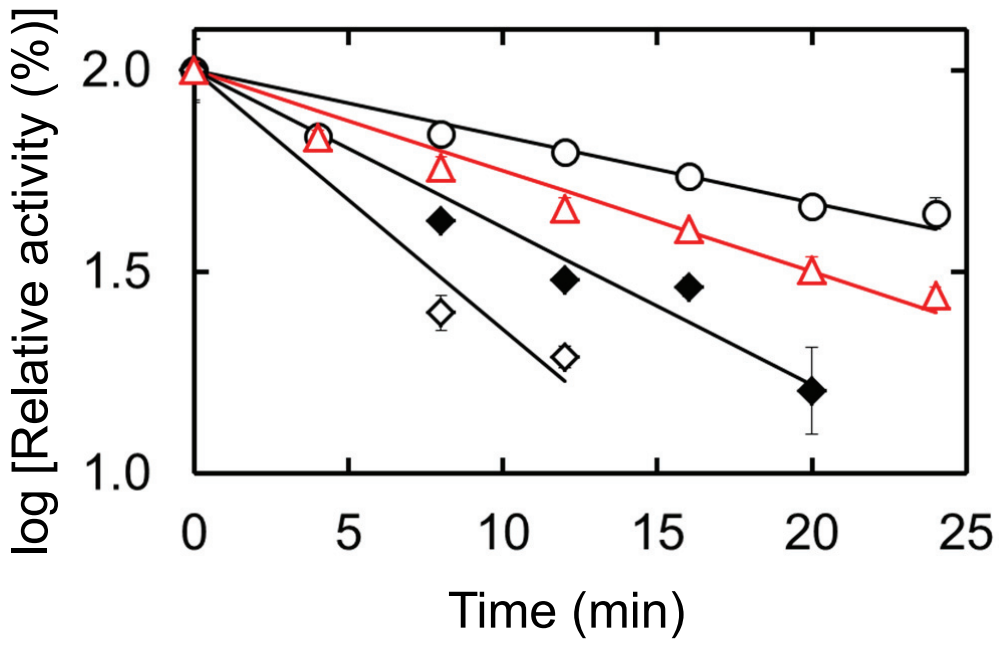

Fig. 5. Thermal inactivation of TLNs. TLN (1 μM) in 40 mM HEPES-NaOH buffer (pH 7.5) containing 10 mM $CaCl_2$ was incubated at 80ºC for 0–24 min. The FAGLA-hydrolytic reaction was carried out with initial concentrations of enzyme and FAGLA of 100 nM and 400 μM respectively at 25ºC. The remaining activity (k_{cat}/K_m) was expressed as the relative value to that of the intact enzyme (WT, 26 mM^{-1} s^{-1}; G117E, 25 mM^{-1} s^{-1}; G117K, 16 mM^{-1} s^{-1}; and G117R, 15 mM^{-1} s^{-1}) and plotted against the incubation time. Symbols: WT (○), G117E (△), G117K (◇), and G117R (◆). Error bars indicate SD values for triplicate measurements.

Chapter 2

Effects of Site-directed Mutagenesis of Asn116 in the β-Hairpin of the N-terminal Domain of Thermolysin on Its Activity and Stability

Introduction

TLN has a β-rich N-terminal domain (Ile1-Asp138) and an α-helical C-terminal domain (Asp150-Lys316) connected by an α-helix (Val139-Thr149) located at the bottom of the active site cleft (Fig. 1) (*10*). Extensive site-directed mutagenesis studies previously conducted in each of the active site polypeptide regions of TLN revealed that the N-terminal sheet and the α-helix 2 are critical to catalysis and the C-terminal loops 1 and 2 are important in substrate recognition (*12*).

Two anti-parallel β-strands, (Asn112-Ala113-Phe114-Trp115 and Ser118-Gln119-Met120-Val121-Tyr122), located in the N-terminal, are connected by an Asn116-Gly117 turn to form a β-hairpin structure (Fig. 2A and B). The Asn112-Trp115 strand is located in the active site and forms the S2′, S1′, and S2 subsites, while the Ser118-Tyr122 strand and the Asn116-Gly117 turn are located outside the active site (*17*). (The subsites and the corresponding residues in the substrates are designated based upon the nomenclature of Schechter, I. and Berger, A. (*48*)). In Chapter 1, it was reported that G117E had higher activity in the hydrolysis of ZDFM but lower activity in the hydrolysis of FAGLA than WT, suggesting that Gly117 plays an important role in substrate specificity. In this study, to explore the catalytic role of the β-hairpin structure and possibly produce a variant enzyme with high performance, we made 19 amino-acid residues substitutions of Asn116 by site-directed mutagenesis and examined their effects on activity and stability.

Materials and Methods

Materials – All materials were prepared as described in Chapter 1.

Bacterial strains, plasmids, and transformation – Expression materials and procedures are as described in Chapter 1. Site-directed mutagenesis, DNA sequencing, transformation, and culturing were performed as described in Chapter 1.

Purification of TLN variants – TLN variants were produced and purified as described in Chapter 1. The concentration of TLN was determined spectrophotometrically using an absorbance value at 277 nm (1 mg/ml) of 1.83 and a molecular mass of 34.6 kDa (*10*).

SDS-PAGE – SDS-PAGE was carried out as described in Chapter 1.

CD measurement – A Jasco J-820 spectropolarimeter (Jasco, Tokyo) equipped with a Peltier system to control the cell temperature was used. The spectrometer conditions were as follows: spectral range 200–260 nm; sensitivity 100 mdeg; resolution 0.1 nm; response time 4 s; scan rate 20 nm min^{-1}; at seven scans per measurement. CD spectra were recorded at 25°C using a 2-mm cell. The concentration of TLN was 1.0 μM in 5 mM Tris-HCl, 10 mM $CaCl_2$, and 0 or 4.0 M NaCl at pH 7.5 (*32, 49*). Because HEPES has high absorbance at 180–210 nm, Tris was used as buffer system (*50*). The control baseline was obtained with solvent and all other the components without TLN. CD spectra were processed with Jasco software, and finally expressed in mean-residue molar ellipticity units, $[\theta]$ (deg cm^2 $dmol^{-1}$).

Hydrolysis of casein – TLN-catalysed hydrolysis of casein was carried out as described in Chapter 1.

Spectrophotometric analysis of the TLN-catalyzed hydrolysis of FAGLA –

TLN-catalysed hydrolysis of FAGLA was carried out as described in Chapter 1.

Spectrophotometric analysis of the TLN-catalyzed hydrolysis of ZDFM – TLN-catalysed hydrolysis of ZDFM was carried out as described in Chapter 1.

Thermal inactivation of TLN – Thermal inactivation of TLN was carried out as described in Chapter 1. However, in this study, TLN was incubated at 80ºC in the presence of 1–100 mM $CaCl_2$ for a specified duration, and the remaining activity that hydrolyzes FAGLA was determined as described above.

Results

Production of Asn116 variants to homogeneity – Asn116 was replaced with either one of the other 19 amino acids. The WT and the variants were expressed in *E. coli* in a system (*15*) in which the mature and pro domains were expressed as independent polypeptides. Figure 3 shows a time-course for a flask-shake culture of the transformants. In all transformants, the OD_{600} of the cultures increased with time and reached a maximum (about 3.0 for the transformant with pUC19 and 1.2–2.3 for the transformants with the expression plasmids for TLN) after 18 or 24 h (Fig. 3A). After the aforementioned duration, in WT, N116A, N116D, N116T, and N116Q, the OD_{600} decreased over time, while in the other 15 variants, it was nearly stable. In WT, N116A, N116D, N116T, and N116Q, casein hydrolysis activity appeared in the supernatant and increased progressively even after OD_{600} reached the maximum level, while in the other 15 variants, it did not appear (Fig. 3B).

Figure 4A and B show the SDS-PAGE of the culture supernatants of the *E. coli* cells transformed with the expression plasmids for WT and the variants. The 34-kDa protein band was clearly detected for WT, N116A, N116D, N116T, and N116Q, but was not for the other 15 variants. Figure 4C shows the SDS-PAGE of the purified preparation of WT, N116A, N116D, N116T, and N116Q. They yielded a single band

with a molecular mass of 34.6 kDa. Table 1 shows the purification data of WT and the four variants. From 450–480 ml of culture supernatants, 0.9–1.6 mg of purified enzymes were obtained. The specific activities of N116A, N116D, N116T, and N116Q in the hydrolysis of casein at 25ºC were 44, 66, 45, and 57%, respectively, of that of WT. Figure 4D shows the CD spectra of the purified enzymes at 200–260 nm. Each spectrum was characterized by negative ellipticities at 202–240 nm with the peaks at about 208 and 225 nm, suggesting that no significant conformational change was occasioned in TLN by the mutations.

Activity of Asn116 variants – Figure 5A shows the pH-dependence of k_{cat}/K_m of the TLN-catalyzed hydrolysis of FAGLA at 25ºC. All plots showed bell-shaped curves with the optimal pH of 6–7. The results are summarized in Table 2. The pK_{e1}, pK_{e2}, and $(k_{cat}/K_m)_o$ values of WT (5.1 ± 0.2, 8.2 ± 0.1, and 37 ± 3 mM^{-1} s^{-1}, respectively) are almost the same as the ones we previously reported (5.3 ± 0.0, 8.3 ± 0.0, and 40 ± 1 mM^{-1} s^{-1}, respectively) (*12*). The $(k_{cat}/K_m)_o$ values of N116D was 320% of that of WT, and those of the other three variants were 70–100% of that of WT. The pK_{e1} and pK_{e2} values of the variants were almost the same as those of WT.

TLN activity increases with increase in concentration of neutral salts (*18*). We defined the degree of the activation as the ratio of the k_{cat}/K_m value with 4.0 M NaCl to that without NaCl, and showed that it is in the range of 13–15 in the hydrolysis of FAGLA (*3, 17, 18*). The k_{cat}/K_m values at pH 7.5 without NaCl and with 4.0 M NaCl and the degree of the activation were 30 ± 4 mM^{-1} s^{-1}, 440 ± 29 mM^{-1} s^{-1}, and 15 for WT, 24 ± 3 mM^{-1} s^{-1}, 330 ± 30 mM^{-1} s^{-1}, and 14 for N116A, 95 ± 4 mM^{-1} s^{-1}, 1000 ± 100 mM^{-1} s^{-1}, and 11 for N116D, 24 ± 1 mM^{-1} s^{-1}, 240 ± 10 mM^{-1} s^{-1}, and 10 for N116T, 31 ± 3 mM^{-1} s^{-1}, 270 ± 40 mM^{-1} s^{-1}, and 9 for N116Q. Thus, the degrees of the NaCl-induced activation of the variants were 60–90% of that of WT.

Figure 5B shows the dependence of the initial reaction rate (v_o) of the TLN-catalyzed hydrolysis of ZDFM on the substrate concentration at pH 7.5, at 25ºC. All plots showed saturated profiles. The kinetic parameters are summarized in Table 3. The K_m values of the variants were 100–130% of that of WT. The k_{cat} value of N116D

was 160% of that of WT, and those of the other three variants were 70–92% of that of WT. The k_{cat}/K_m value of N116D was 140% of that of WT, and those of other three variants were 60–100%. These results indicate that N116D has higher activity than WT. They also indicate that N116Q has similar activity as WT, and N116A and N116T have reduced activities.

Stability of Asn116 variants – We examined time-dependences of the thermal inactivation of WT and the variants at 80°C in the presence of various concentrations of $CaCl_2$ ranging 1–100 mM. All inactivations followed pseudo-first-order kinetics (Fig. 6A for 10 mM $CaCl_2$, data not shown for 1, 30, 50, and 100 mM $CaCl_2$). Figure 6B shows k_{obs} of WT and the variants at each $CaCl_2$ concentration. They decreased with increasing $CaCl_2$ concentrations and were in the order N116A, N116D, N116T > N116Q > WT at all $CaCl_2$ concentrations examined.

Discussion

Catalytic role of Asn116 – Figure 7A shows the typical β-hairpin peptide backbone with two amino acid residues (t1 and t2) at the turn (*51*). The most common t1 and t2 residues are Asn and Gly, respectively, followed by Gly and Ser. Thus, we can ascribe not only Asn116 and Gly117 to t1 and t2 residues, but also Gly117 and Ser118 can be ascribed, respectively. Figure 2A is a close-up view of the polypeptide Asn112-Tyr122, in which side chains of all residues are shown. It appears the side chains of Trp115, Asn116, and Val121 are located inside the β-plane formed by the Asn112-Trp115 and Ser118-Tyr122 β-strands, while those of other residues are located outside it. The carbonyl oxygen (OD1) of Asn116 is involved in two hydrogen bonds, one with the main-chain nitrogen (N) of Ser118 and the other with N of Gln119. Such hydrogen bonds are absent in the typical β-hairpin peptide backbone (Fig. 7A). Figure 2B is another close-up view of the polypeptide Asn112-Tyr122, in which side chains of Trp115, Asn116, and Val121 are shown. It appears that there are two β-planes, one

formed by the polypeptides Asn112-Trp115 and Met120-Tyr122 and the other formed by Trp115-Met120. The side chain of Asn116 is located in the β-plane formed by Trp115-Met120, while those of Trp115 and Val121 are outside of these two β-planes. This is in contrast to recent reports that the Trp-Trp interaction between the two β strands is important for the stability of β-hairpin structure (*52–54*). Figure 2C shows an illustration of the two β-plane structure formed by the polypeptide Asn112-Tyr122. Such structure is absent in the typical β-hairpin peptide backbone (Fig. 7A).

In this study, we used an *E. coli* expression system which does not require autocatalytic cleavage: the mature domain and the pre-prodomain of TLN were co-expressed constitutively as independent polypeptides under the original promoter sequences in the *npr* gene, which encodes TLN (*34*). Previously we reported that all 70 variants, in which one of twelve active-site residues (Ala113, Phe114, Trp115, Asp150, Tyr157, Gly162, Ile168, Ser169, Asp170, Asn227, Val230, and Ser234) was replaced with either Asp, Glu, His, Lys, Arg, or Ala, could be produced at similar levels by this expression system whether or not they retained activity (*12*). In this study, of the 19 Asn116 variants, only four were produced (Figs. 3 and 4). The reason N116A, N116D, N116T, and N116Q are active and the other 15 variants are inactive is unclear. However, there are interesting features: only amino acid residues with side chains of moderate size can be accommodated inside the β-hairpin structure and are favorable at position 116.

In the hydrolysis of FAGLA and ZDFM, the activities were in the order N116D > WT > N116Q > N116A, N116T (Fig. 5). In thermal treatment, the stabilities were in the order WT > N116Q > N116D, N116T, N116A (Fig. 6). These results suggest that Asn116 plays an important role in the activity and stability of TLN presumably by stabilizing the β-hairpin structure. It is not clear why N116D is more active than WT. Relating to this, we previously speculated into the reason the TLN variant L144S was more active than WT: the side chain of Leu144 is buried in the interior of the protein, and thus the activation by these mutations is due to an increase in flexibility of TLN by a decrease in density of the inner part of the molecule (*31*). If this is true for N116D, the activation by the mutation of Asn116→Asp might be due to an increase in flexibility of TLN by the change in electrostatic environment of the β-hairpin structure.

It is interesting to note that N116D is more active but less stable than N116Q. This might be explained by the trade-off between activity and stability in enzymes: mutations which increase activity are accompanied with decrease in stability and vice versa (*32, 55, 56*).

The degree of the salt-induced activation of N116D was 11, comparable to that of WT (15). This suggests that salt-induced activation in TLN cannot be replaced by introducing activating mutations in place Asn116. This is in contrast to our previous finding that the degree of activation of highly active variants, L144S and D150E, were 4 and 5, respectively, and that salt-induced activation might be replaceable to some extent (*32*).

Role of the AsnGly sequence in the β-hairpin structure in zinc-proteinases – Figure 7B shows the amino acid sequences of the β-structured polypeptides of five zinc-proteinases, *Bacillus cereus* neutral protease (*57*), *Pseudomonas aeruginosa* elastase (*58*), vibryolysin (*59*), protealysin (*60*), and human angiotensin I-converting enzyme (*61*), corresponding to Asn112-Tyr122 of TLN. The amino acid residues corresponding to Asn112, Ala113, Phe114, Trp115, Gly117, Ser118, and Met120 of TLN are highly conserved. In their crystal structures (Protein Data Bank accession number: *B. cereus* neutral protease, 1ESP; *P. aeruginosa* elastase, 3DBK; vibryolysin, 3NQY; protealysin, 2VQX; and human angiotensin I-converting enzyme, 1UZE), we noticed two hydrogen bonds in each of the five zinc-proteinases, corresponding to that between OD1 of Asn116 and N of Ser118 and that between OD1 of Asn 116 and N of Gln119 of TLN. They are the hydrogen bond between OD1 of Asn117 and N of Ser 119 and that between OD1 of Asn117 and N of Gln120 for *B. cereus* neutral protease, that between OD1 of Asp116 and N of Ser118 and that between OD1 of Asp116 and N of Ala119 for *P. aeruginosa* elastase, that between OD1 of Asp321 and N of Ser323 and that between OD1 of Asp 321 and N of Ala324 for vibryolysin, that between OD1 of Asn136 and N of Gln138 and that between OD1 of Asn136 and N of Gln139 for protealysin, and that between OD1 of Asn361 and N of Lys363 and that between OD1 of Asn361 and N of Asp364 for human angiotensin I-converting enzyme. This revealed

that the AsnGly or AspGly sequence and the hydrogen bonds between the OD1 of the Asn or Asp residue at the position of *i* and the N of the residues at *i+1* and *i+2* are well conserved in zinc-proteinases.

It is presumed that the carbonyl oxygen of the introduced Asp (OD1 or OD2) and Gln (OD1) forms the same hydrogen bonds as OD1 of Asn116 does. This presumption is supported by the observation that in *P. aeruginosa* elastase, the carbonyl oxygen of Asp116 forms the hydrogen bonds with the main-chain nitrogen of Thr118 and that of Ala119 (Fig. 7D). However, it should be noted that N116A has activity in spite of the fact that the introduced Ala116 does not form such hydrogen bonds. Therefore, we think that those hydrogen bonds are important for activity, but are not indispensable.

In conclusion, a highly active TLN variant N116D was obtained. It is suggested that Asn116 plays an important role in the activity and stability of TLN presumably by stabilizing the β-hairpin structure. Site-directed mutagenesis of analogous residues in the β-hairpin structure might be similarly effective in improving performances in various zinc-proteinases.

Table 1. Purification of Asn116 variants from the supernatant of the *E. coli* transformants.

WT	Volume (ml)	Activity (units)	Recovery (%)	Protein (mg)	Specific activity (units/mg)	Purification (fold)
Culture supernatant	450	59,000	100	54	1,100	1.0
Phenyl chromatography	180	34,000	58	8.8	3,800	3.4
Affinity chromatography	7.8	11,000	19	0.9	12,000	11

N116A	Volume (ml)	Activity (units)	Recovery (%)	Protein (mg)	Specific activity (units/mg)	Purification (fold)
Culture supernatant	480	51,000	100	67	760	1.0
Phenyl chromatography	150	21,000	41	12	1,800	2.3
Affinity chromatography	9.1	8,500	17	1.6	5,300	7.0

N116D	Volume (ml)	Activity (units)	Recovery (%)	Protein (mg)	Specific activity (units/mg)	Purification (fold)
Culture supernatant	480	54,000	100	68	790	1.0
Phenyl chromatography	180	27,000	50	13	2,100	2.7
Affinity chromatography	11	11,000	20	1.4	7,900	10

N116T	Volume (ml)	Activity (units)	Recovery (%)	Protein (mg)	Specific activity (units/mg)	Purification (fold)
Culture supernatant	460	41,000	100	74	550	1.0
Phenyl chromatography	170	21,000	51	13	1,600	2.9
Affinity chromatography	10	8,600	21	1.6	5,400	9.8

N116Q	Volume (ml)	Activity (units)	Recovery (%)	Protein (mg)	Specific activity (units/mg)	Purification (fold)
Culture supernatant	480	46,000	100	49	940	1.0
Phenyl chromatography	180	30,000	65	14	2,100	2.2
Affinity chromatography	7.5	6,800	15	1.0	6,800	7.2

Table 2. pK_e and intrinsic k_{cat}/K_m ($(k_{cat}/K_m)_o$) values of Asn116 variants in the hydrolysis of FAGLA at 25°C.

TLN	pK_{e1}	pK_{e2}	$(k_{cat}/K_m)_o$ (mM^{-1} s^{-1})
WT	5.1 ± 0.2 (0.0)	8.2 ± 0.1 (0.0)	37 ± 3 (1.0)
N116A	5.1 ± 0.1 (±0.0)	8.3 ± 0.1 (+0.1)	31 ± 1 (0.8)
N116D	5.4 ± 0.1 (+0.3)	8.4 ± 0.1 (+0.2)	117 ± 6 (3.2)
N116T	5.1 ± 0.1 (±0.0)	8.5 ± 0.1 (+0.3)	26 ± 1 (0.7)
N116Q	5.1 ± 0.2 (±0.0)	8.3 ± 0.1 (+0.1)	37 ± 3 (1.0)

Average of triplicate determinations with SD values are shown. Numbers in parentheses indicate ΔpK_e compared to those of WT and the $(k_{cat}/K_m)_o$ relative to that of WT.

Table 3. Kinetic parameters of Asn116 variants in the hydrolysis of ZDFM at 25ºC.

TLN	K_m (mM)	k_{cat} (s^{-1})	k_{cat}/K_m (mM^{-1} s^{-1})
WT	0.39 ± 0.04 (1.0)	7.7 ± 0.1 (1.0)	20 ± 1 (1.0)
N116A	0.41 ± 0.04 (1.1)	6.7 ± 0.7 (0.8)	16 ± 1 (0.8)
N116D	0.43 ± 0.04 (1.1)	12 ± 1 (1.5)	27 ± 2 (1.4)
N116T	0.49 ± 0.03 (1.3)	5.4 ± 0.1 (0.7)	11 ± 1 (0.6)
N116Q	0.38 ± 0.06 (1.0)	7.1 ± 0.1 (0.9)	19 ± 1 (1.0)

Average of triplicate determinations with SD value is shown. Numbers in parentheses indicate values relative to those of WT.

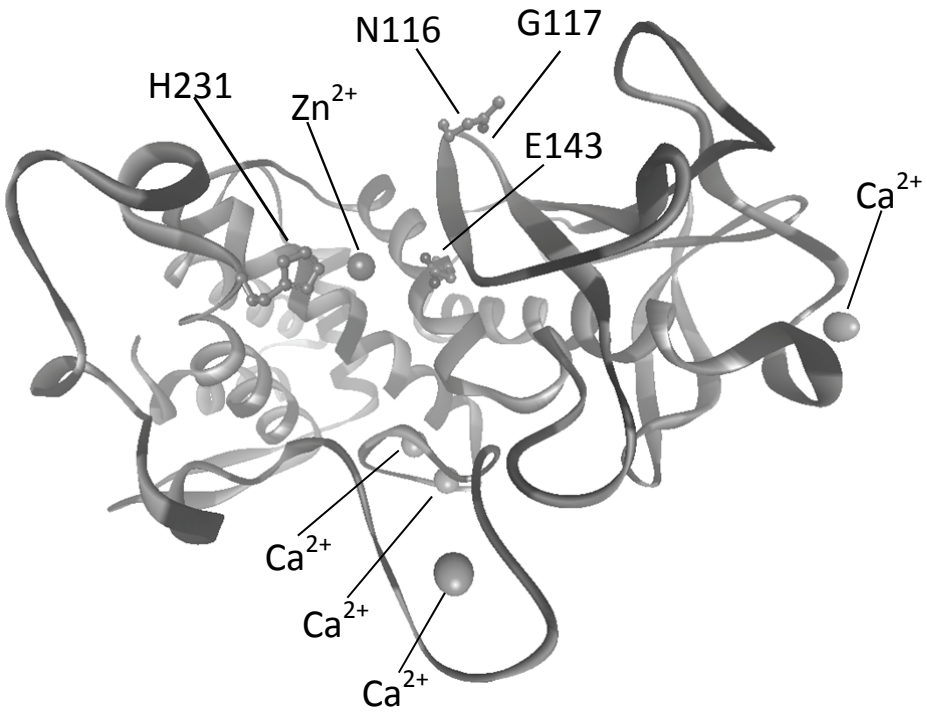

Fig. 1. Overall structure of TLN. The structure is based on Protein Data Bank accession number 8TLN. The main chain is represented by a ribbon model. Side chains of Asn116 and Gly117 and the catalytically important residues Glu143 and His231 are shown by a ball and stick. Zinc and calcium ions are shown as spheres.

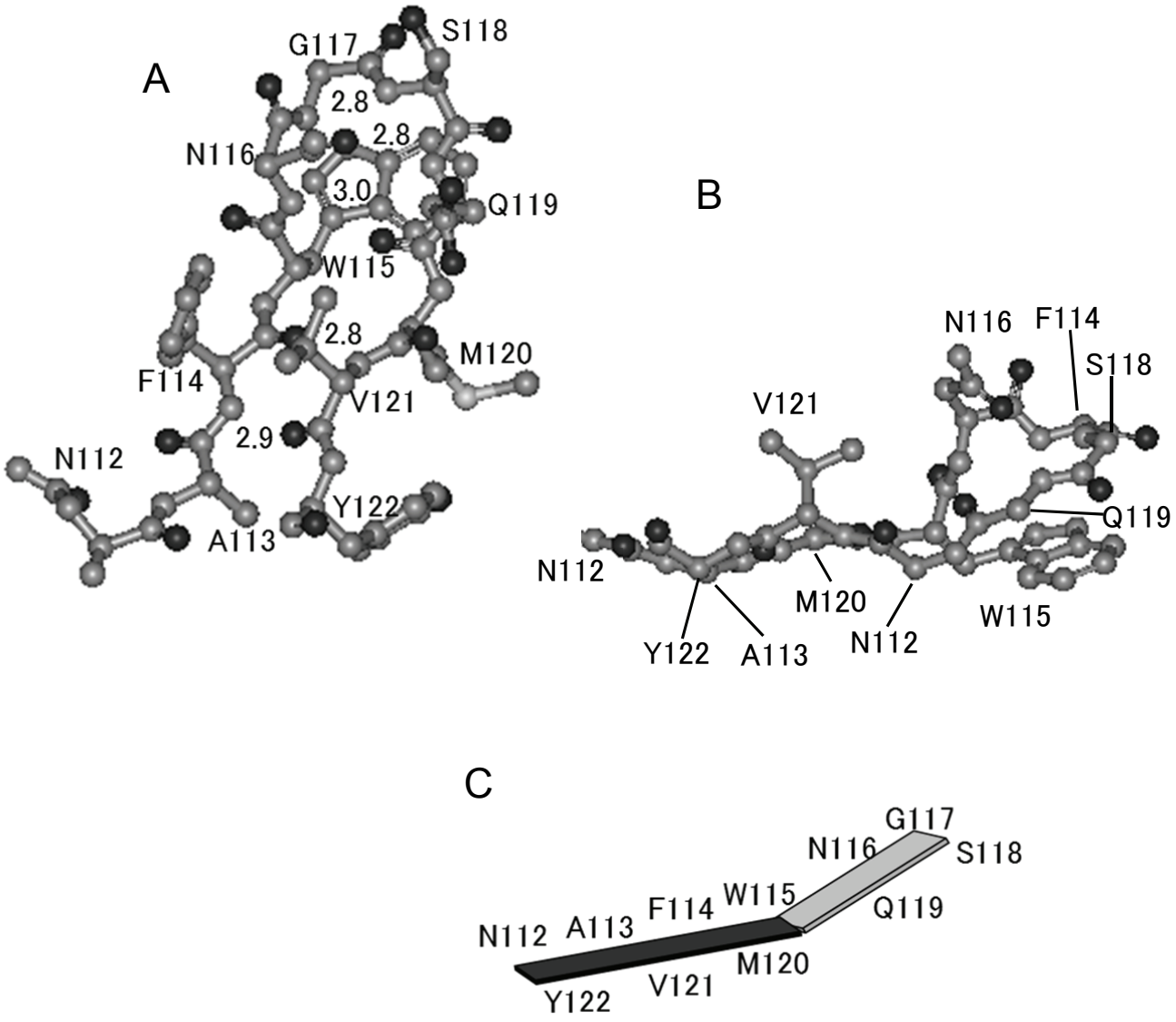

Fig. 2. β-Hairpin structure in TLN active site. (A) and (B), Close-up view of the Asn112-Trp115 strand, the Asn116-Gly117 loop, and the Ser118-Tyr122 strand of TLN. All atoms are shown by a ball and stick (A), and all main-chain atoms and the side-chain atoms of Trp115, Asn116, and Val121 are shown by a ball and stick (B). Oxygen is colored black, and carbon, nitrogen, and sulfur gray. Hydrogen bonds are represented by dotted lines together with the distances (Å). (C) Illustration of the two β-planes formed by Asn112-Trp115 and Met120-Tyr122 and by Trp115-Met120.

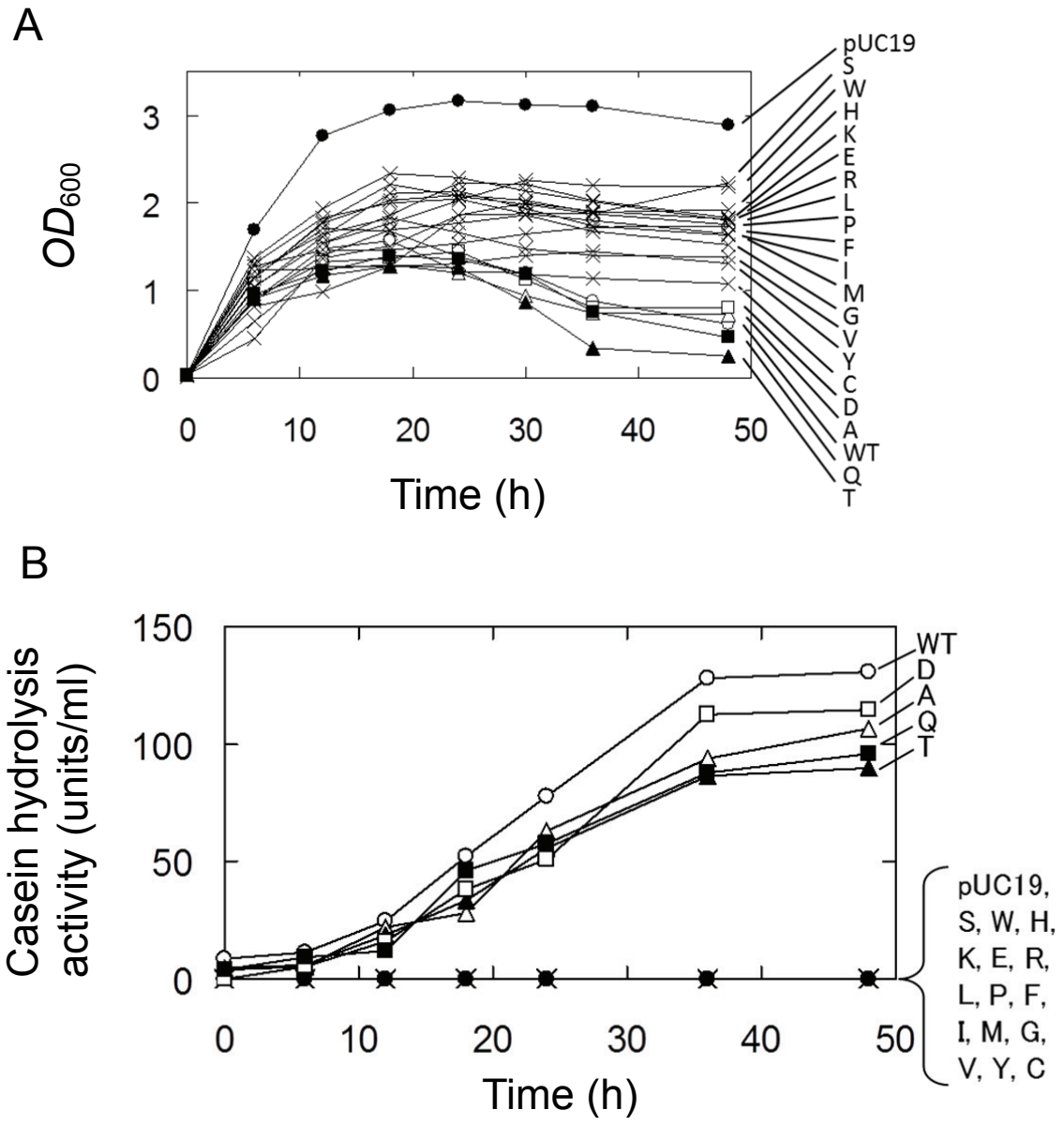

Fig. 3. Culturing of *E. coli*. (A) Cell densities. (B) Casein hydrolysis activities. OD_{600} of culture (A) and casein hydrolysis activities of the supernatants (B) of *E. coli* cells transformed with pUC19 (●) or the expression plasmids for WT (○), N116A (Δ), N116D (□), N116T (▲), N116Q, (■), or the other 15 variants (+) are plotted against time. In the figure, the points of the 15 variants are overlapped with those of pUC19. 0 h means start of flask-shake culture. Variant names are abbreviated: for example, "A" stands for N116A.

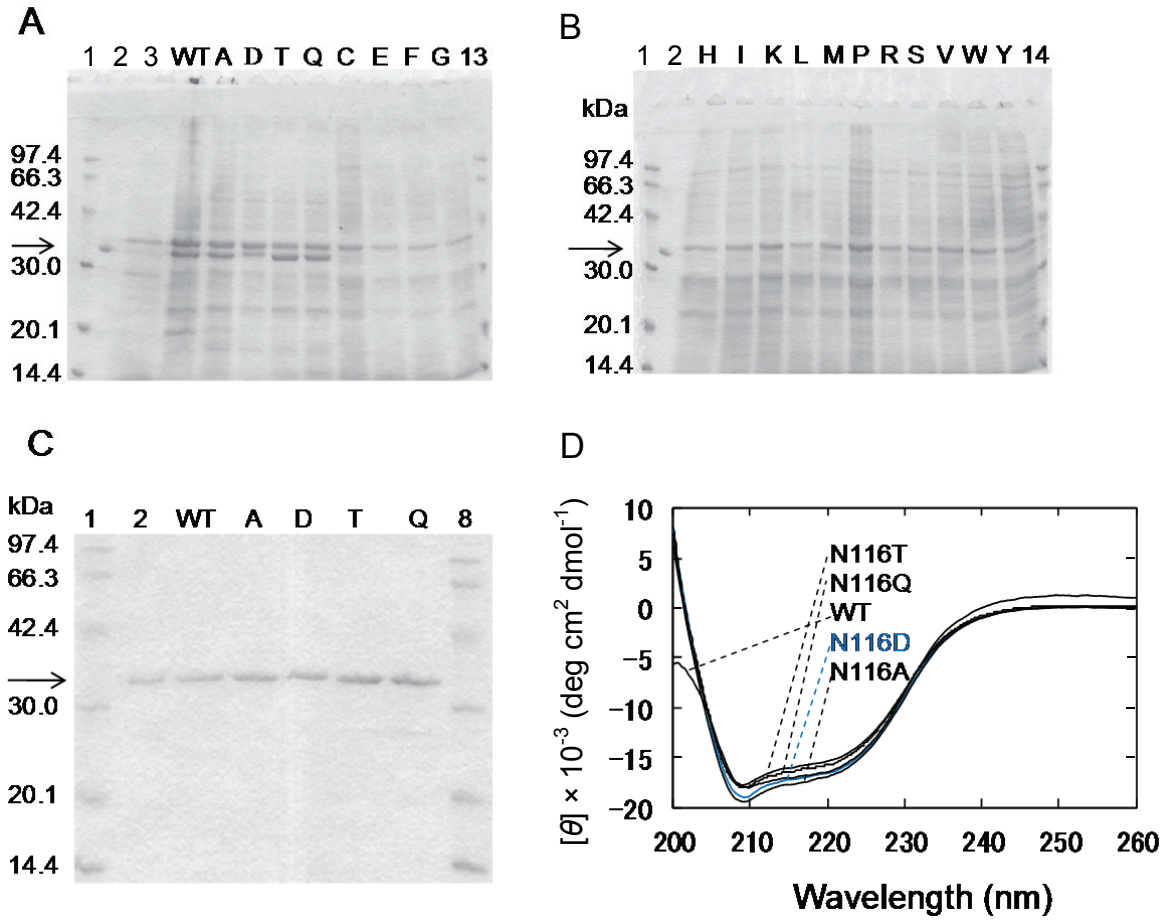

Fig. 4. Expression and purification of Asn116 variants. (A-C) Coomassie Brilliant Blue-stained 12.5% SDS-PAGE. (A) The marker proteins (lanes 1 and 13), native TLN purified from *B. thermoproteolyticus* (lane 2), and the supernatants of *E. coli* cells transformed with pUC-19 (lane 3) and the expression plasmids for WT (lane WT), N116A (lane A), N116D (lane D), N116T (lane T), N116Q (lane Q), N116C (lane C), N116E (lane E), N116F (lane F), N116G (lane G). (B) The marker proteins (lanes 1 and 14), native TLN purified from *B. thermoproteolyticus* (lane 2), and the supernatants of *E. coli* cells transformed with the expression plasmids for N116H (lane H), N116I (lane I), and N116K (lane K), N116L (lane L), N116M (lane M), N116P (lane P), N116R (lane R), N116S (lane S), N116V (lane V), N116W (lane W), and N116Y (lane Y). (C) The marker proteins (lanes 1 and 8), native TLN purified from *B. thermoproteolyticus* (lane 2), and purified preparations of WT (lane WT), N116A (lane A), N116D (lane D), N116T (lane T), and N116Q (lane Q). The arrow indicates the band corresponding to TLN. (D) CD spectra. CD spectra were measured for 2.1 μM TLN in 5 mM Tris-HCl, 10 mM $CaCl_2$ at pH 7.5, at 25ºC.

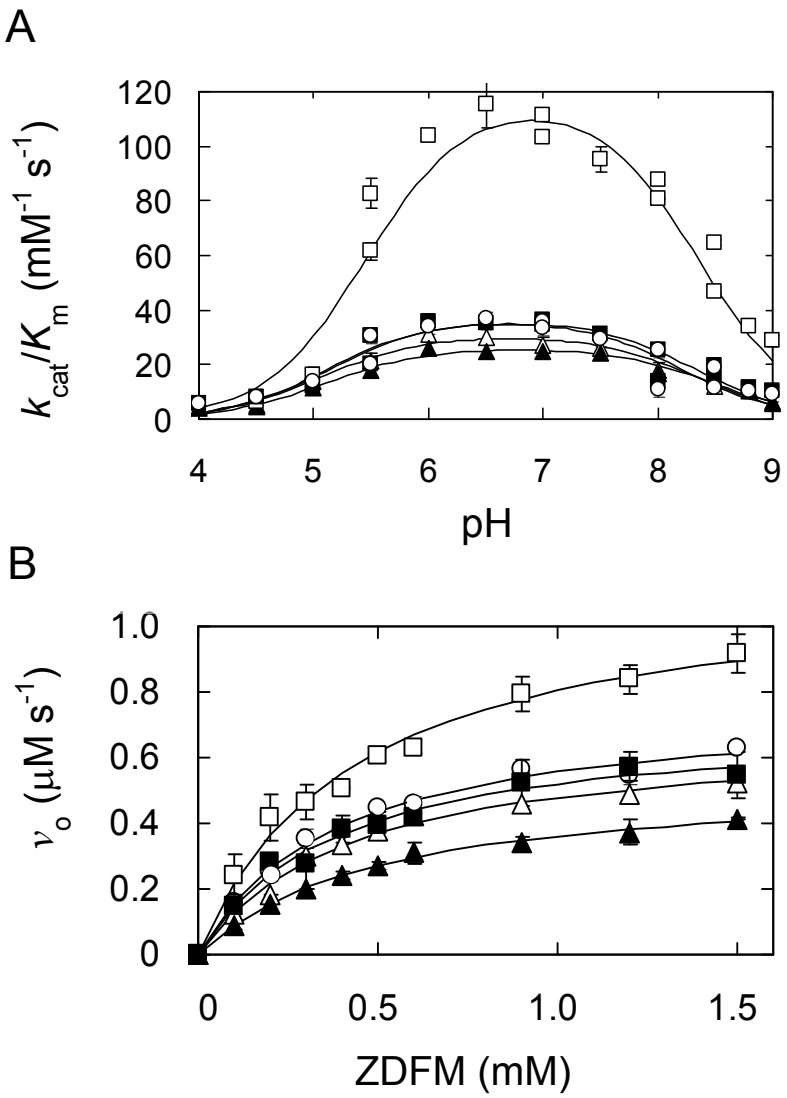

Fig. 5. Activity of Asn116 variants. (A) Effect of pH on the initial reaction rate (v_o) in the hydrolysis of FAGLA. The reaction was carried out in 40 mM acetate-NaOH at pH 4.0–5.5, 40 mM MES-NaOH at pH 5.5–7.0, 40 mM HEPES-NaOH at pH 7.0–8.5, and 40 mM TAPS-NaOH at pH 8.0–9.0, each of which contained 10 mM $CaCl_2$, at 25ºC. The initial concentrations of enzyme and FAGLA were 100 nM and 400 μM, respectively. (B) Dependence of v_o on substrate concentration in the hydrolysis of ZDFM. The reaction was carried out in 40 mM Tris-HCl, 10 mM $CaCl_2$ at pH 7.5, at 25ºC. Symbols for enzymes: WT (○), N116A (Δ), N116D (□), N116T (▲), and N116Q (■). Error bars indicate SD values for three-times measurements.

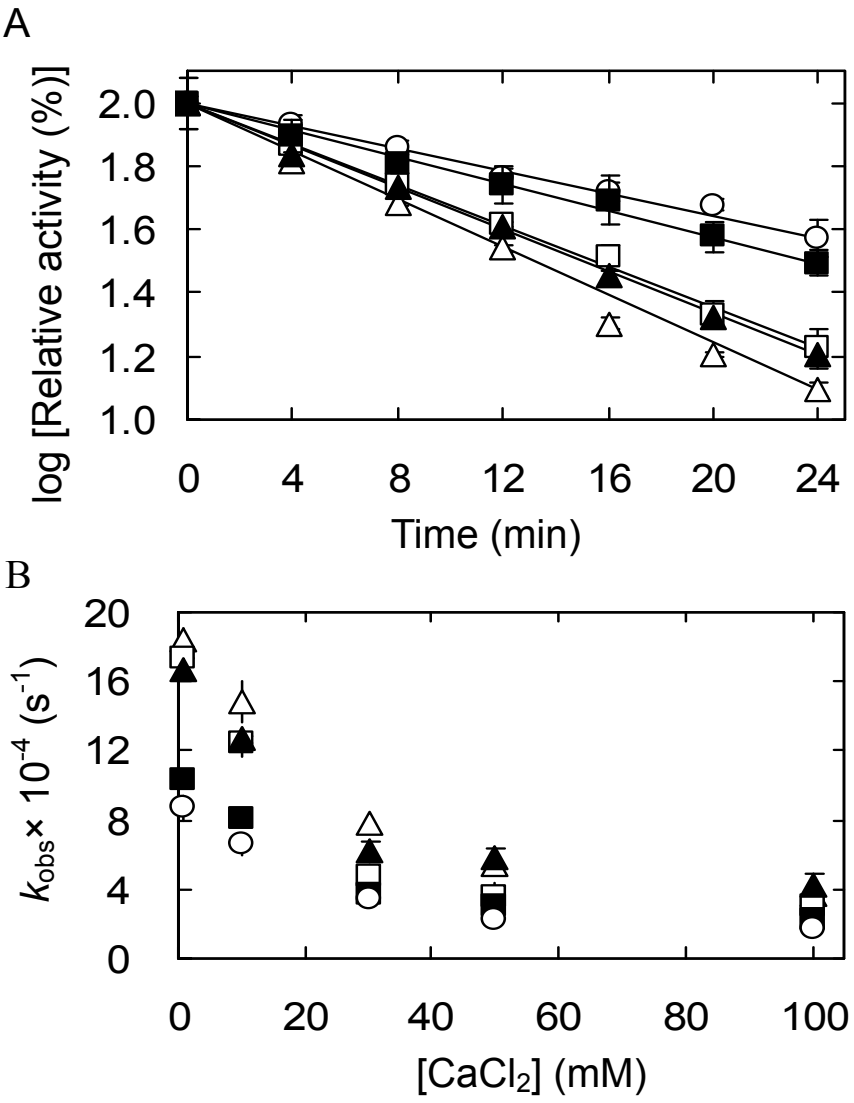

Fig. 6. Thermal stability of Asn116 variants. (A) Thermal inactivation at 10 mM $CaCl_2$. (B) Effect of $CaCl_2$ concentration on the thermal inactivation. TLN (2 μM) in 40 mM HEPES-NaOH, 1, 10, 30, 50, or 100 mM $CaCl_2$ at pH 7.5 was incubated at 80ºC for a specified duration. The FAGLA-hydrolytic reaction was carried out at 25ºC with the initial concentrations of enzyme and FAGLA of 100 nM and 400 μM, respectively. The remaining activity (k_{cat}/K_m) was expressed as the relative value to that of the intact enzyme (WT, 29 mM^{-1} s^{-1}; N116A, 23 mM^{-1} s^{-1}; N116D, 95 mM^{-1} s^{-1}; N116T, 23 mM^{-1} s^{-1}; and N116Q, 29 mM^{-1} s^{-1}) and plotted against the incubation time (A). The k_{obs} values of TLN were plotted against the $CaCl_2$ concentration (B). Symbols correspond to those of Fig. 5. Error bars indicate SD values for three-times measurements.

A

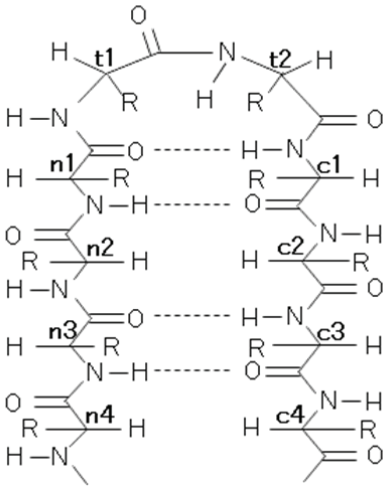

B

Enzyme	Sequences
TLN	112 N A F W N G S Q M V Y 122
B. cereus neutral protease	113 N A F W N G S Q M Y Y 123
P. aeruginosa elastase	112 N A Y W D G T A M L F 122
Vibryolysin	317 N A F W D G S A M T F 327
Protealysin	132 N A F W N G Q Q M V F 142
Human antigotensin I-converting enzyme	357 W D F Y N G K D F R I 367

C

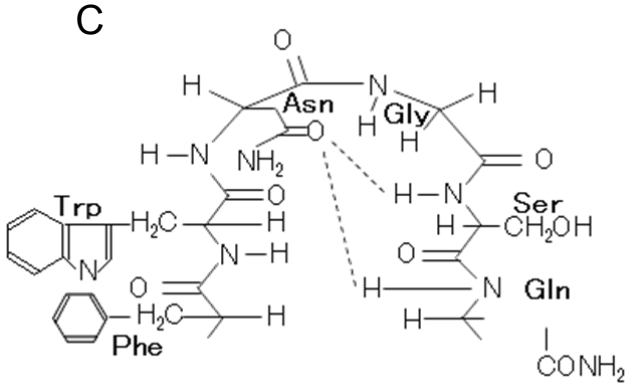

TLN and *B. cereus* neutral protease

D

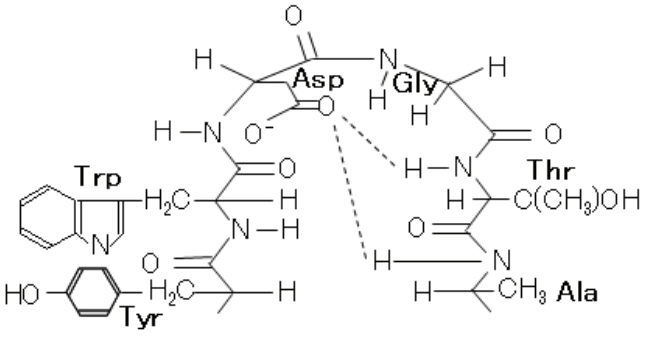

P. aeruginosa elastase

Fig. 7. β-hairpin structure. (A) Schematic illustration of typical β-hairpin peptide backbone with two amino acid residues at the turn. Side chains are indicated by "R". Hydrogen bonds linking the amide hydrogen and carbonyl oxygen are indicated by dotted lines. Residues at the N-terminal β-strand, at the turn, and at the C-terminal β-strand are labelled turn as "n", "t", and "c", respectively. (B) Amino acid sequences of zinc-proteinases corresponding to Asn112-Tyr122 of TLN. (C) Schematic illustration of the β-hairpin structures of Phe114-Gln119 of TLN and Phe115-Gln120 of *B. cereus* neutral protease. (D) Schematic illustration of the β-hairpin structure of Tyr114-Ala119 of *P. aeruginosa* elastase.

Chapter 3

Effects of the Mutations, Asn116 to Asp and Asp150 to Glu, of Thermolysin on Its Salt-induced Activation and Stabilization

Introduction

TLN activity increases in an exponential fashion with increasing concentration of neutral salts (*17, 18, 20–23*). TLN stability also increases at 0–2 M NaCl (*9*). This stabilizing effect decreases above 2 M NaCl (*20*). Previously, several mutations which increase the hydrolytic activity for FAGLA and ZDFM were identified (*12*, *31*, *Chapter 1*, *Chapter 2*). Of such mutations, Asn116→Asp (*Chapter 2*) and Asp150→Glu (*12*) exhibited the highest effect. In the absence of NaCl, the activities of N116D and D150E are about 3 times higher than that of WT (*12, Chapter 2*). In the absence of NaCl, Asn116→Asp decreased stability while Asp150→Glu did not change it. Asn116 is located in the β-hairpin structure in the N-terminal domain, while Asp150 is located in the active-site loop in the C-terminal domain (Fig. 1). Out of the 19 variants of Asn116, only N116D exhibited higher activity than WT while maintaining a high level of NaCl-induced activation comparable to that of WT (*Chapter 2*). This was unique in comparison to our earlier work wherein variants with higher activity than WT, such as D150E, exhibited drastically reduced degrees of NaCl-induced activation (*12*).

In this study, to explore the mechanism of the salt-induced activation and stabilization of TLN, we compared the effects of Asn116→Asp and Asp150→Glu on NaCl-induced activation and stabilization. The results indicate that Asp150→Glu markedly decreases NaCl-induced activation and stabilization while Asn116→Asp does not exhibit any such marked decrease. Based on the results obtained, we discuss the mechanism of the salt-induced activation and stabilization of TLN.

Materials and Methods

Materials – All materials were prepared as described in Chapter 1.

Bacterial strains, plasmids, and transformation – Expression materials and procedures are as described in Chapter 1. Site-directed mutagenesis, DNA sequencing, transformation, and culturing were performed as described in Chapter 1.

Purification of TLN – TLN variants were produced and purified as described in Chapter 1.

SDS-PAGE – SDS-PAGE was carried out as described in Chapter 1.

Hydrolysis of casein – TLN-catalysed hydrolysis of casein was carried out as described in Chapter 1.

Spectrophotometric analysis of the TLN-catalyzed hydrolysis of FAGLA – TLN-catalysed hydrolysis of FAGLA was carried out as described in Chapter 1.

Spectrophotometric analysis of the TLN-catalyzed hydrolysis of ZDFM – TLN-catalysed hydrolysis of ZDFM was carried out as described in Chapter 1.

CD measurement – CD measurement was carried out as described in Chapter 2.

Thermal inactivation of TLN – Thermal inactivation of TLN was essentially carried out as described in Chapter 1. However, in this study, TLN solutions containing 0–4.0 M NaCl was incubated at 70ºC for specified durations, and the remaining activity to hydrolyze FAGLA was determined as described above.

Results

Production of TLN variants – Starting with 500 ml of *E. coli* cultures, 0.7–2.0 mg of purified preparations of TLN variants were recovered (Table 1). On SDS-PAGE under reducing conditions, each of them yielded a single band with a molecular mass of 34.6 kDa (Fig. 2). All CD spectra of WT and variants measured in the presence of 0 and of 4.0 M NaCl were essentially the same: each spectrum was characterized by negative ellipticities at about 206–230 nm with peaks at about 208 and 225 nm (data not shown). This suggests that no significant conformational change was occasioned in TLN by mutation and/or 4.0 M NaCl. Table 1 shows the hydrolysis activities of the TLN variants for casein at pH 7.5 at 25ºC. The activities of the variants relative to that of WT were 60–70%. This indicates that the mutations of Asn116→Asp and Asp150→Glu decrease casein-hydrolyzing activity, in accord with our previous results (*12, 23, 34*).

NaCl-induced activation of TLN variants in FAGLA hydrolysis – The FAGLA-hydrolyzing activities of WT and its variants in the presence of 0–4.0 M NaCl were measured (Fig. 3). The k_{cat}/K_m values in the absence of NaCl were $(2.8 \pm 0.3) \times 10^4$ M^{-1} s^{-1} for WT, in good accord with that reported previously [$(2.9 \pm 0.2) \times 10^4$ M^{-1} s^{-1}] (*32*), $(9.2 \pm 1.2) \times 10^4$ M^{-1} s^{-1} for N116D, $(7.5 \pm 0.1) \times 10^4$ M^{-1} s^{-1} for D150E, and $(1.6 \pm 0.2) \times 10^5$ M^{-1} s^{-1} for N116D/D150E. This indicates that the mutations Asn116→Asp and Asp150→Glu increase FAGLA-hydrolyzing activity, and the Asn116→Asp in combination with Asp150→Glu yielded a significant increase in the hydrolytic activity of FAGLA. The k_{cat}/K_m values of WT and the variants increased with increasing NaCl concentrations in an exponential fashion. Relative activity was defined by eq. 1:

$$\text{Relative activity at x M NaCl} = \frac{k_{cat}/K_m \text{ at x M NaCl}}{k_{cat}/K_m \text{ at 0 M NaCl}} \qquad (1)$$

The relative activity at 0–4.0 M of WT was expressed by $y = 1.97^x$ (y is the

relative activity at x M NaCl); the y value is in good agreement with that (1.9) reported previously (*18*), and those of N116D, D150E, and N116D/D150E were expressed by $y = 1.75^x$, $y = 1.49^x$, and $y = 1.46^x$, respectively. The degrees of activation at 4.0 M NaCl were 15 for WT, 9.3 for N116D, 4.9 for D150E, and 4.5 for N116D/D150E, and the k_{cat}/K_m values were $(4.3 \pm 0.4) \times 10^5$, $(8.6 \pm 0.7) \times 10^5$, $(3.7 \pm 0.2) \times 10^5$, and $(7.4 \pm 0.7) \times 10^5$ M^{-1} s^{-1}, respectively. These indicate the relative activities at 0.5–4.0 M NaCl at pH 7.5 were in the order WT > N116D > D150E, N116D/D150E. In other words, Asp150→Glu markedly reduced NaCl-induced activation, while Asn116→Asp reduced it slightly.

Figure 4A and B shows the effects of pH on the FAGLA-hydrolysis activity of WT and the variants at 25ºC at 0 and 4.0 M NaCl, respectively. All the plots showed bell-shaped curves, with an optimal pH of about 7. The acidic and alkaline pK_e (pK_{e1} and pK_{e2}) values and the $(k_{cat}/K_m)_o$ values are summarized in Table 2. In WT, the pK_{e1} value shifted from 5.2 to 6.4 while the pK_{e2} value remained constant at 4.0 M NaCl, in good accord with those reported previously (*21*). The pK_{e1} and pK_{e2} values of the variants were almost the same as those of WT. The $(k_{cat}/K_m)_o$ values of N116D and N116D/D150E were higher than those of WT both at 0 and at 4.0 M NaCl. The $(k_{cat}/K_m)_o$ value of D150E was higher than that of WT at 0 M NaCl, but was almost the same at 4.0 M NaCl. Figure 4C shows the effects of pH on the relative activity at 4.0 M NaCl of WT and the variants in the hydrolysis of FAGLA. All the plots show bell-shaped curves with maximum activation at pH 7.5. The relative activities at 4.0 M NaCl at pH 6.0−9.0 were in the order WT > N116D > D150E, N116D/D150E.

NaCl-induced activation of TLN variants in ZDFM hydrolysis – ZDFM is a precursor of the artificial sweetener aspartame. TLN catalyzes its formation from *N*-carbobenzoxy-L-aspartic acid and L-phenylalanine methyl ester through reverse reaction of hydrolysis. Table 3 shows the kinetic parameters at 0 and 4.0 M NaCl of WT and the variants in the hydrolysis of ZDFM. The k_{cat} value of WT increased from 5.3 to 39 s^{-1} while the K_m value remained constant, in good accord with those reported previously (*18*). Similar results were obtained for the variants. The relative activity at

4.0 M NaCl was in the order WT > N116D > D150E, N116D/D150E.

NaCl-induced stabilization of TLN variants – The thermal inactivation of the TLN variants at 70°C in the presence of 10 mM $CaCl_2$ and 0–4.0 M NaCl was examined. Inactivation of all the variants followed pseudo-first-order kinetics pattern (data not shown). The k_{obs} values in the absence of NaCl were $(3.4 \pm 0.3) \times 10^{-4}$ s^{-1} for WT, in good accord with that reported previously [$(3.9 \pm 0.3) \times 10^{-4}$ s^{-1}] (*31*), $(6.4 \pm 0.2) \times 10^{-4}$ s^{-1} for N116D, $(3.2 \pm 0.5) \times 10^{-4}$ s^{-1} for D150E, and $(6.8 \pm 0.9) \times 10^{-4}$ s^{-1} for N116D/D150E. This indicates that mutation Asn116→Asp decreases stability, while Asp150→Glu does not affect it. Relative stability was defined by eq. 2:

$$\text{Relative stability at x M NaCl} = \frac{k_{obs} \text{ at 0 M NaCl}}{k_{obs} \text{ at x M NaCl}} \quad (2)$$

The relative stabilities are plotted in Fig. 5. The k_{obs} values of WT and the variants decreased at 0.5–1.0 M NaCl but increased with increasing NaCl concentrations from 1.0 to 4.0 M. The relative stabilities at 0.5–1.0 M NaCl of D150E and N116D/D150E were lower than those of WT and N116D, respectively, and those of N116D were higher than those of WT. This indicates that Asp150→Glu reduced NaCl-induced stabilization and that Asn116→Asp enhanced it.

Discussion

Insight into the mechanism of NaCl-induced activation of TLN – The degree of NaCl-induced activation was in the order WT > N116D > D150E, N116D/D150E (Figs. 3 and 4C, Tables 2 and 3), indicating that Asp150→Glu markedly and Asn116→Asp slightly reduced NaCl-induced activation. All the variants exhibited pH-activity profiles similar to WT both at 0 and at 4.0 M NaCl (Fig. 4A and B). NaCl-induced activation of WT and the variants was brought by the increase in k_{cat} values, while the K_m values

remained constant (Table 3). These results indicate that mutations Asn116→Asp and Asp150→Glu affect the mechanism of NaCl-induced activation of TLN, however they have no effect on the catalytic mechanism.

Because the content of free water in a solution with such high concentrations of NaCl (1–4.0 M) is low, the dielectric constant must be low (*17, 18*). However, the order of ions as to efficiency in the activation of TLN ($Na^+ > K^+ > Li^+$) is different from the Hofmeister series which corresponds to the degree of hydration of ions ($Li^+ > Na^+ > K^+$) (*17, 18, 20–23*). This is in contrast to the case of human immunodeficiency virus type-1 (HIV-1) protease, in which activation is same as in the Hofmeister series (*62, 63*). Based on this evidence, we have pointed out that salt-induced activation of TLN cannot be explained only by a reduction in dielectric constant of the reaction medium, and that it is in part the result of direct interactions of enzyme molecules with ions (*17*, *18*, *21–23*).

Mutation Asp150→Glu increases activity (*Chapter 1*). In this study, this mutation reduced NaCl-induced activation (Fig. 3), indicating that salt-induced activation was replaced by Asp150→Glu to some extent. Asp150 is located in the loop of the C-terminal domain, Asp150-Gly162. This loop connects two α-helices in the active site, Val139-Thr149 and Ala163-Val176. The former contains catalytically important residues Glu143 and two zinc-chelating residues, His142 and His146, and the latter contains one zinc-chelating residue, Glu166. Crystallographic studies of complexes of TLN with representative inhibitors *N*-(α-L-rhamnopyranosyl-oxyhydroxyphosphinyl)-L-leucyl-L-tryptophan (phosphoramidon) and *N*-phosphoryl-L-leucinamide (*P*-Leu-NH_2) have revealed that no residue in this C-terminal loop is involved in the binding of phosphoramidon or *P*-Leu-NH_2 (*64*), suggesting that the loop is not involved in substrate binding. In view of this, we advance the possibility that the binding of certain residues in this loop with ions is important for the salt-induced activation of TLN.

The mechanism of NaCl-induced stabilization of TLN – We have indicated that TLN is more stable at 0.5–1.5 M NaCl than at 0 or 2.0–4.0 M (*20*). This suggests that the effect of NaCl on stability is attributable to an increased conformational stability of

TLN as a result of its preferential hydration. In this study, mutation Asp150→Glu reduced NaCl-induced stabilization, while Asn116→Asp enhanced it (Fig. 4). This indicates that salt-induced stabilization is diminished by Asp150→Glu to some extent. This does not exclude the stabilizing effect of neutral salts in reducing the dielectric constant of the reaction medium, but the possibility that certain residues in this loop bind with ions cannot be ruled out. Thermal inactivation of TLN is associated with autolysis (*65, 66*). Therefore, the apparent decrease in stability above 2.0 M NaCl is attributable to an increase in activity and the simultaneous enhancement of autolysis.

Characteristics of TLN compared with other halophilic enzymes – Enzymes that are activated or stabilized by neutral salts are termed halophilic (*67*). Crystallographic and site-directed mutagenesis studies of halophilic enzymes have revealed the mechanisms of hallophilicity. Malate dehydrogenase from *Halobacterium marismortui* is an active tetramer above 2 M NaCl or KCl, but an inactive monomer below 2 M, and the binding of Lys205 with a chloride ion is responsible for dimerization (*68*). The nucleotide diphosphate kinase from *Halobacterium salinarum* is an active tetramer in the presence of sodium ions and an inactive dimer in its absence, and Glu134 is responsible for the formation of a tetramer (*69*). Human angiotensin-converting enzyme changes the position of an active-site loop in the presence of NaCl, and the binding of three Arg residues (Arg186, Arg489, and Arg522) with one chloride ion is responsible for this activation (*70*).

It appears that the mechanisms of salt-induced activation and stabilization of TLN are different from those of the halophilic enzymes mentioned above. As noted (*20, 23*), the halophilic properties of TLN are different as between activity and stability. In this study, we found that the effects of mutations on the NaCl-induced activation and stabilization of TLN vary depending on species of mutation. Our results suggest that the binding of ions with certain residues is important in the salt-induced activation and stabilization of TLN. It is difficult to identify such residues by crystallographic analysis of TLN (*71*). Although it is also difficult to predict the effects of mutations on TLN structure, we think that the characterization of salt-induced activation and stabilization

of a number of TLN variants aid in estimating those residues.

Table 1. Purification of TLN variants from the supernatants of the *E. coli* transformants.

	Volume (ml)	Activity (units)	Recovery (%)	Protein (mg)	Specific activity (units/mg)	Purification (fold)
WT						
Culture supernatant	400	58,000	100	40	1,500	1.0
Phenyl chromatography	280	27,000	46	11	2,500	1.7
Affinity chromatography	6	14,000	24	1	14,000	9.3
N116D						
Culture supernatant	390	59,000	100	70	840	1.0
Phenyl chromatography	250	27,000	46	15	1,800	2.1
Affinity chromatography	5.5	6,800	12	0.8	8,500	10
D150E						
Culture supernatant	460	57,000	100	46	1,200	1.0
Phenyl chromatography	280	47,000	82	11	4,300	3.6
Affinity chromatography	5.5	7,200	13	0.7	10,000	8.3
N116D/D150E						
Culture supernatant	330	84,000	100	61	1,400	1.0
Phenyl chromatography	280	64,000	76	9	7,100	5.0
Affinity chromatography	5	20,000	24	2	10,000	7.0

Table 2. pK_e and intrinsic k_{cat}/K_m [$(k_{cat}/K_m)_o$] values of TLN variants in the hydrolysis of FAGLA at 25ºC.

	pK_{e1}	pK_{e2}	$(k_{cat}/K_m)_o$ x 10^{-4} (M^{-1} s^{-1})
i) 0 M NaCl			
WT	5.2 ± 0.1 (0.0)	8.3 ± 0.1 (0.0)	3.7 ± 0.2 (1.0)
N116D	5.3 ± 0.1 (+0.1)	8.4 ± 0.1 (+0.1)	11 ± 1 (2.9)
D150E	5.2 ± 0.1 (0.0)	8.2 ± 0.1 (-0.1)	9.5 ± 0.3 (2.6)
N116D/D150E	5.4 ± 0.1 (+0.2)	8.3 ± 0.1 (0.0)	19 ± 1 (5.1)
ii) 4.0 M NaCl			
WT	6.4 ± 0.1 (0.0)	7.9 ± 0.1 (0.0)	56 ± 3 (1.0)
N116D	6.4 ± 0.1 (0.0)	8.1 ± 0.1 (+0.2)	140 ± 10 (2.5)
D150E	6.4 ± 0.1 (0.0)	7.8 ± 0.1 (-0.1)	59 ± 6 (1.1)
N116D/D150E	6.5 ± 0.1 (+0.1)	8.1 ± 0.1 (+0.2)	110 ± 10 (2.0)

Numbers in parentheses indicate ΔpK_e as compared to those of WT and the $(k_{cat}/K_m)_o$ relative to that of WT. Average of triplicate determinations with SD values are shown.

Table 3. Salt-induced activation of TLN variants in the hydrolysis of ZDFM at 25ºC.

	$K_m \times 10^{-4}$ (M)		k_{cat} (s^{-1})	
	0 M NaCl	4 M NaCl	0 M NaCl	4 M NaCl
WT	3.8 ± 0.4 (1.0)	3.7 ± 0.4 (1.0)	5.3 ± 0.2 (1.0)	39 ± 1 (1.0)
N116D	4.3 ± 0.5 (1.1)	4.2 ± 0.5 (1.1)	11 ± 1 (2.0)	54 ± 3 (1.4)
D150E	4.3 ± 0.5 (1.1)	4.4 ± 0.8 (1.2)	16 ± 1 (3.0)	45 ± 4 (1.2)
N116D/D150E	4.3 ± 0.7 (1.1)	4.3 ± 0.7 (1.2)	19 ± 1 (3.6)	50 ± 3 (1.3)

	$k_{cat}/K_m \times 10^{-4}$ (M^{-1} s^{-1})		Relative activity at 4 M NaCl
	0 M NaCl (A)	4 M NaCl (B)	B/A
WT	1.4 ± 0.2 (1.0)	11 ± 1 (1.0)	7.9 (1.0)
N116D	2.4 ± 0.3 (1.7)	13 ± 1 (1.2)	5.4 (0.7)
D150E	3.6 ± 0.5 (2.6)	10 ± 1 (0.9)	2.8 (0.4)
N116D/D150E	4.5 ± 0.7 (3.2)	12 ± 1 (1.1)	2.7 (0.3)

The reaction was carried out in 40 mM HEPES-NaOH buffer at pH 7.5 containing 10 mM $CaCl_2$, 0 or 4.0 M NaCl at 25ºC. The initial concentrations of TLN and ZDFM were 0.1 μM and 0.1–1.5 mM, respectively. Numbers in parentheses indicate values relative to those of WT. Average of duplicate determination with SD value is shown.

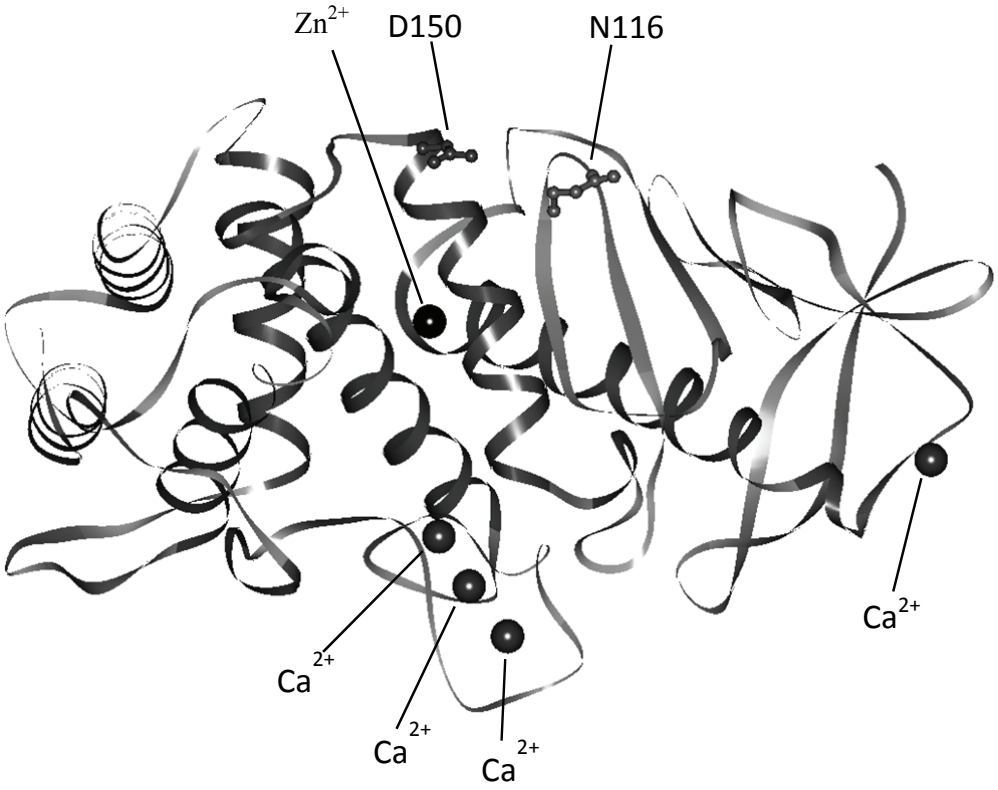

Fig. 1. Whole structure of TLN. The structure is based on PDB code 8TLN (*9*). The overall protein structure (ribbon model), the mutated residues (Asn116 and Asp150) (ball and stick model), and zinc and calcium ions (sphere) are shown.

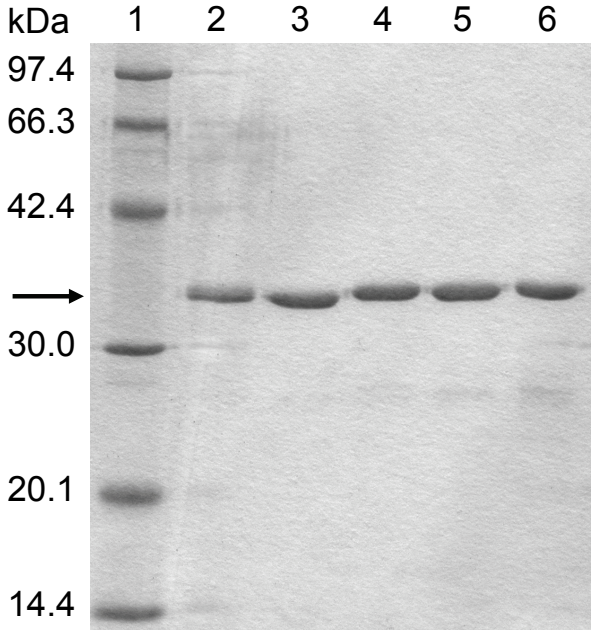

Fig. 2. SDS-PAGE of TLN variants. Coomassie Brilliant Blue-stained 12.5% SDS-polyacrylamide gel is shown. Purified preparations (1.2 μg) were applied to each lane. Lane 1, molecular-mass marker; lane 2, native TLN purified from *B. thermoproteoliticus*; lane 3, WT; lane 4, N116D; lane 5, D150E; and lane 6, N116D/D150E. The arrow indicates the position of TLN.

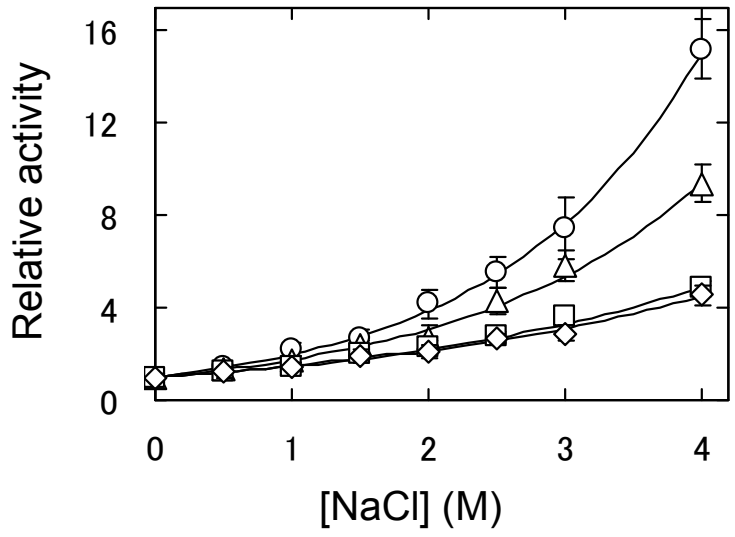

Fig. 3. Effect of NaCl concentration on the FAGLA-hydrolysis activity of TLN variants. The reaction was carried out in 40 mM HEPES buffer at pH 7.5 containing 10 mM $CaCl_2$, 0–4.0 M NaCl at 25°C. The initial concentrations of enzyme and FAGLA were 0.1 μM and 400 μM, respectively. The relative activity of TLN variants was defined as the ratio of the k_{cat}/K_m value at x M NaCl to that at 0 M NaCl [$(2.8 \pm 0.3) \times 10^4$ M^{-1} s^{-1} for WT, $(9.2 \pm 1.2) \times 10^4$ M^{-1} s^{-1} for N116D, $(7.5 \pm 0.1) \times 10^4$ M^{-1} s^{-1} for D150E, and $(1.6 \pm 0.2) \times 10^5$ M^{-1} s^{-1} for N116D/D150E]. The solid line represents a theoretical curve by $y = 1.97^x$ (y is the relative activity at x M NaCl) for WT, that by $y = 1.75^x$ for N116D, that by $y = 1.49^x$ for D150E, and that by $y = 1.46^x$ for N116E/D150E, which are drawn to fit the experimental data. Symbols: WT (○), N116D (Δ), D150E (□), and N116D/D150E (◇). Error bars indicate SD values of triplicate measurements.

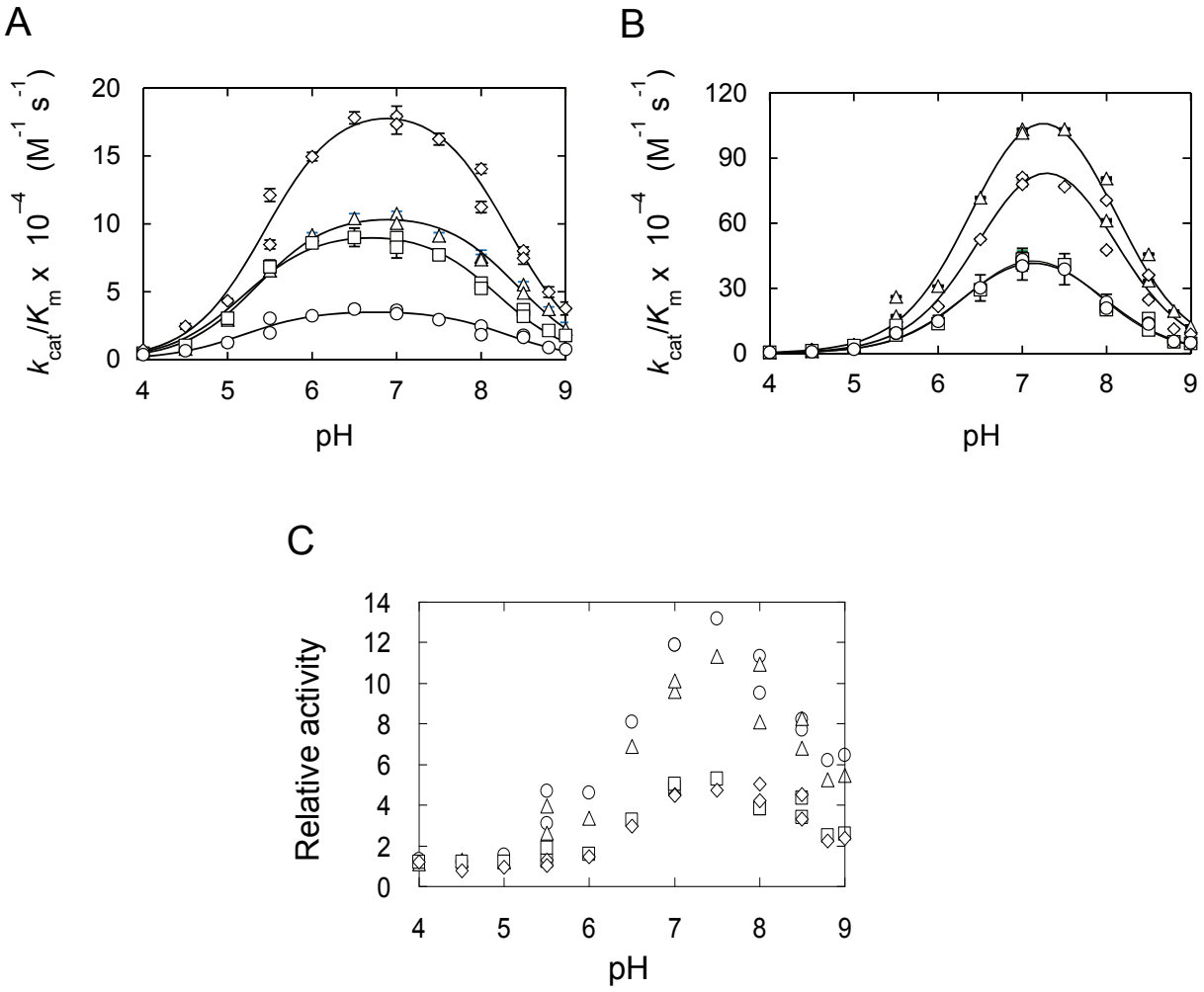

Fig. 4. Effect of pH on the FAGLA-hydrolysis activity of TLN variants. The reaction was carried out in 40 mM acetate-NaOH buffer at pH 4.0-5.5, 40 mM MES-NaOH buffer at pH 5.5-7.0, 40 mM HEPES-NaOH buffer at pH 7.0-8.5, and TAPS-NaOH buffer at pH 8.0-9.0, containing 10 mM $CaCl_2$ at 25ºC in the absence or presence of 4.0 M NaCl. The initial concentrations of enzyme and FAGLA were 0.1 μM and 400 μM, respectively. (A) Effect of pH on k_{cat}/K_m at 0 M NaCl. (B) Effect of pH on k_{cat}/K_m at 4.0 M NaCl. (C) Effect of pH on the relative activity at 4.0 M NaCl. Symbols correspond to those of Fig. 3. Error bars indicate SD values of triplicate measurements.

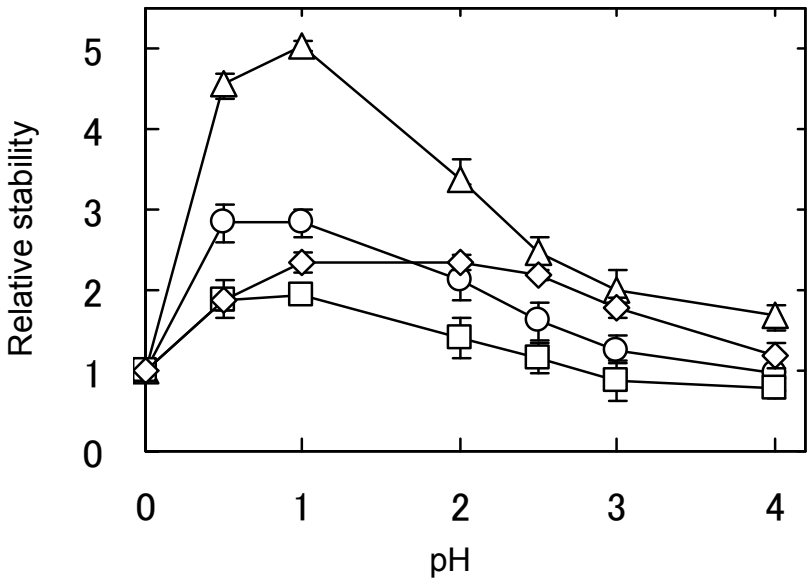

Fig. 5. Effect of NaCl concentration on the thermal stability of TLN variants. TLN (2.0 μM) in 40 mM HEPES-NaOH, 10 mM $CaCl_2$, 0–4.0 M NaCl at pH 7.5 was incubated at 70°C for a specified time. The experimental condition for FAGLA hydrolysis corresponds to that of Fig. 3. The relative stability of TLN variants was defined as the ratio of the k_{obs} at 0 M NaCl [$(3.4 \pm 0.3) \times 10^{-4}$ s^{-1} for WT, $(6.4 \pm 0.2) \times 10^{-4}$ s^{-1} for N116D, $(3.2 \pm 0.5) \times 10^{-4}$ s^{-1} for D150E, and $(6.8 \pm 0.9) \times 10^{-4}$ s^{-1} for N116D/D150E] to that at x M NaCl. Symbols correspond to those of Fig. 3. Error bars SD values of triplicate measurements.

Chapter 4

Effects of Conversion of the Zinc-binding Motif Sequence of Thermolysin, HEXXH, to That of Dipeptidyl Peptidase III, HEXXXH, on the Activity and Stability of Thermolysin

Introduction

Dipeptidyl peptidase III (DPP III) [EC 3.4.14.4] is a mesophilic zinc metalloproteinase. It was originally identified in the bovine anterior pituitary gland (*72*). Human (*73*) and rat (*74*) DPP III enzymes consist of 737 and 738 amino acid residues respectively. Unlike most zinc metalloproteinases, DPP III has the zinc-binding motif sequence $H^{450}ELLGH^{455}$. DPP III releases N-terminal dipeptides sequentially from a peptide. In rat DPP III, two histidine residues (His450 and His455) in the sequence and one glutamate residue (Glu508) chelate the active-site Zn^{2+}, and Glu451 in the sequence is critical to catalytic activity (*75*). DPP III is grouped in the M49 family of Clan MA. It has been identified in a wide range of organisms, from bacteria to humans, and all of these contain the zinc-binding motif HEXXXH (*76*), indicating that DPP III is a typical evolutionarily conserved protein.

In DPP III, replacement of the active-site Zn^{2+} with Cu^{2+}, Co^{2+}, or Ni^{2+} does not affect activity much (*77*). In TLN, replacement of the active-site Zn^{2+} with Cd^{2+}, Mn^{2+}, or Fe^{2+} abolishes or decreases activity, while replacement with Co^{2+} increases it (*66, 65, 78–80*). In DPP III, conversion of zinc-binding motif sequence $H^{450}ELLGH^{455}$ to one similar to that of TLN, $H^{450}ELGH^{455}$, does not affect enzymatic activity (*75*). In the DPP III variant with $H^{450}ELGH^{455}$, unlike the wild-type DPP III, replacement of the active-site Zn^{2+} with Cu^{2+}, Co^{2+}, or Ni^{2+} abolishes activity (*81*).

In TLN and other zinc metalloproteinases, the effects of conversion of zinc-binding motif sequence HEXXH to HEXXXH on catalytic activity have not been

characterized. In this study, we examined the effects of this conversion on the activity and stability of TLN. The results indicate that this conversion eliminates TLN activity but does not affect substrate analog-binding ability or stability.

Materials and Methods

Materials – All materials were prepared as described in Chapter 1.

Bacterial strains, plasmids, and transformation – Expression materials and procedures are as described in Chapter 1. Site-directed mutagenesis, DNA sequencing, transformation, and culturing were performed as described in Chapter 1.

Purification of TLN variants – The cells were harvested at 20,000 × *g* for 20 min, then suspended in 3 ml of 20 mM acetate-NaOH buffer (pH 5.5) and 10 mM $CaCl_2$ (buffer A), and disrupted by sonication. After centrifugation at 20,000 × *g* for 20 min, the supernatant was collected and applied to a column (internal diameter 10 mm x 50 mm) of Gly-D-Phe coupled to CNB-activated Sepharose 4B resin (GE Healthcare, Buckinghamshire, UK) equilibrated with buffer A. TLN variants were eluted with buffer A containing 20% (v/v) 2-propanol and 2.5 M NaCl at a flow rate of 1 ml/min.

SDS-PAGE – SDS-PAGE was carried out as described in Chapter 1.

Hydrolysis of casein – TLN-catalysed hydrolysis of casein was carried out as described in Chapter 1.

Spectrophotometric analysis of the TLN-catalyzed hydrolysis of FAGLA – TLN-catalysed hydrolysis of FAGLA was essentially carried out as described in Chapter 1. However, in this study, TLN solution (0.2 ml) containing soluble fractions corresponding to 3 ml of culture medium were added to 2.8 ml of a solution containing

4 mM FAGLA in 40 mM HEPES-NaOH, 10 mM $CaCl_2$ (buffer B), pH 7.5 at 25ºC, and incubated at 25°C for one min. To determine the effects of various concentrations of Zn^{2+} and of Co^{2+} on activity, a TLN solution (0.2 ml) containing purified TLN preparations (2 μM) and various concentrations of $ZnCl_2$ (0–500 μM) or $CoCl_2$ (0–2 mM) were pre-incubated for 1 h on ice and added to 3.8 ml of a solution containing 0.421 mM FAGLA in buffer B. During the reaction, the decrease in A_{345} of the reaction solution was measured. The amount of FAGLA hydrolyzed was evaluated as described in Chapter 1.

CD measurement – CD measurement was carried out as described in Chapter 2.

Structural modelling – For modelling of the modified TLNs, an iterative threading assembly refinement server, I-TASSER was used. I-TASSER queries a given sequence and generates 3D structural models from multiple threading alignments in PDB (*84–87*). Assessment of the structural models was done with C-score (1.67), TM score (0.95 ± 0.05), and RMSD (1.1 ± 1.1Å). The model presented was found to be the best, and was validated by PROCHECK and Verify_3D using the U.S. National Institutes of Health (NIH) server.

Results

Design of TLN variants with zinc-binding motif sequence HEXXXH – We designed $H^{142}ELLGH^{146}$ and $H^{142}ELTGH^{146}$ as altered zinc-binding motif sequences that belong to the HEXXXH motif. The former is the same as the sequence of DPP III. The latter has a glycine residue between Thr145 and His146 of the sequence of TLN, $H^{142}ELTH^{146}$. It appears that the flexibility conferred by Gly454 enables DPP III to hold the active-site Zn^{2+}, but the possibility that Gly145b impairs the active-site geometry of TLN cannot be discounted. A TLN variant with $H^{142}ELLGH^{146}$ is designated T145LG, and one with $H^{142}ELTGH^{146}$ is designated T145TG.

Figure 1A shows the structure of WT, based on PDB code 8TLN. Figure 1B shows the modeled structure of T145TG. Unlike WT, the turn of the α-helix that contains $H^{142}ELTGH^{146}$ is extended, suggesting that this might not enable His146 to be coordinated to the active-site Zn^{2+}. This is in contrast to DPP III, in which the turn of the α-helix that contains $H^{450}ELLGH^{455}$ is widened (Fig. 1C), suggesting that this enables both His450 and His455 to be coordinated to the active-site Zn^{2+} (*81*). As Fig. 1 also shows, in TLN the side-chains of Tyr84 and Val140 are located between two α helices, Ala68-Asn89 and Val139-Thr149. The mutation Tyr84→Ser or Val140→Ala was aimed at reducing the sizes of the side-chains, anticipating that this reduction would enable the widening of the turn of the α-helix Val139-Thr149 of T145LG and T145TG. Here the TLN variant with Tyr84→Ser is designated Y84S; that with Val140→Ala is V140A; that with Tyr84→Ser and $H^{142}ELTH^{146}$→$H^{142}ELLGH^{146}$ is Y84S/T145LG; that with Val140→Ala and $H^{142}ELTH^{146}$→$H^{142}ELLGH^{146}$ is V140A/T145LG; that with Tyr84→Ser and $H^{142}ELTH^{146}$→$H^{142}ELTGH^{146}$ is Y84S/T145TG; and that with Val140→Ala and $H^{142}ELTH^{146}$→$H^{142}ELTGH^{146}$ is V140A/T145TG.

Expression of TLN variants – WT and the variants were expressed in *E. coli* by a system reported previously (*34*), one in which the mature and pro domains were expressed as independent polypeptides. Figure 2 shows a time course for a flask-shake culture of the transformants. In all the transformants, the OD_{600} of the cultures increased with time and reached a maximum (about 2.2 for the transformant with pUC19, and about 0.8−2.0 for the transformants with expression plasmids for TLN) after 18−30 h (Fig. 2A). After the aforementioned durations, in WT and V140A, the OD_{600} decreased with time, and in the other six variants (Y84S, T145LG, Y84S/T145LG, V140A/T145LG, T145TG, Y84S/T145TG, and V140A/T145TG), it was almost stable. The casein hydrolysis activities of WT and V140A were detected in the supernatant, and increased progressively even after OD_{600} reached maximum, but was not detected for the seven other variants (Fig. 2B). These results indicate that the conversion of Tyr84 to Ser and that of $H^{142}ELTH^{146}$ to $H^{142}ELLGH^{146}$ or $H^{142}ELTGH^{146}$ eliminate TLN activity, while that of Val140 to Ala does not eliminate it.

Figure 3A shows SDS-PAGE of the culture supernatants of the transformed *E. coli* cells with the expression plasmids for WT and the variants. The 34.6-kDa protein band was detected for WT and V140A but not for the seven other variants. This suggests that TLN is secreted by leakage from the cytosol into the culture medium due to hydrolysis of membrane proteins by active TLN. Figure 3B shows SDS-PAGE of the soluble fractions of the *E. coli* cells transformed with the expression plasmids for WT and the variants. The 34.6-kDa protein band was detected for WT and all eight variants. These results indicate that none of the conversions of Tyr84 to Ser, Val140 to Ala, or $H^{142}ELTH^{146}$ to $H^{142}ELLGH^{146}$ or $H^{142}ELTGH^{146}$ affected the expression of TLN in *E. coli*.

Activity of TLN variants – Because WT and all the variants were expressed in soluble fractions of the transformed *E. coli* cells, their hydrolysis activities were examined. First the casein hydrolysis activities of a solution containing 2.5% (v/v) soluble fractions were measured at pH 7.5 at 25ºC. The activities of WT and V140A were 232 ± 13 and 248 ± 12 units/ml respectively, while those of the other variants were not detected. Next, the FAGLA hydrolysis activities of a solution containing 6.7% (v/v) soluble fractions were measured at pH 7.5 at 25ºC. The activities of WT and V140A were 178 ± 10 and 198 ± 9 nM s^{-1} respectively, while those of the other variants were not detected. These results indicate that the conversion of Tyr84 to Ser and of $H^{142}ELTH^{146}$ to $H^{142}ELLGH^{146}$ or $H^{142}ELTGH^{146}$ abolished TLN activity while that of Val140 to Ala did not abolish it.

Substrate analog-binding ability of the TLN variants – We examined the binding abilities of variants for the substrate analog Gly-D-Phe. Figure 4A and B show SDS-PAGE of the pass-through and eluted fractions, respectively, of Gly-D-Phe column chromatography of the soluble fractions of the transformed *E. coli* cells. In WT and all the variants, the 34.6-kDa protein band was not detected in the pass-through fractions for WT or any variant (Fig. 4A), but it was detected in the eluted fractions (Fig. 4B), indicating that none of the conversion of Tyr84 to Ser, Val140 to Ala, or of $H^{142}ELTH^{146}$

to $H^{142}ELLGH^{146}$ or $H^{142}ELTGH^{146}$ affected the binding ability of TLN for Gly-D-Phe.

Purification of TLN variants – Starting with 450 ml of *E. coli* cultures, 0.6–1.0 mg of purified preparations of WT, T145LG, and T145TG were recovered by hydrophobic-interaction column chromatography and Gly-D-Phe affinity column chromatography of the soluble fractions of the transformed *E. coli* cells. On SDS-PAGE under reducing conditions, each of these yielded a single band with a molecular mass of 34.6 kDa (Fig. 5A). On far-UV CD spectroscopy at 25°C, all of them exhibited negative ellipticities at about 203–238 nm, with the peaks at about 208 and 222 nm (Fig. 5B). This suggests that T145LG and T145TG did not suffer any drastic structural changes by the conversion of $H^{142}ELTH^{146}$ to $H^{142}ELLGH^{146}$ and $H^{142}ELTGH^{146}$ respectively. Noting that Tyr84 is close to the modified site, near-UV CD spectroscopy was carried out to discern any changes in the tertiary structure of the protein near the active site (Fig. 5C). No significant change was observed, suggesting that the environment of the aromatic side-chains of Tyr84 of T145LG and T145TG were not altered by conversion of the zinc-binding motif sequence.

Stability of the TLN variants – We examined the thermal denaturation of WT, T145LG, and T145TG by monitoring θ_{222} in the range 75–95°C (Fig. 6). All the denaturation curves exhibited an apparent two-state model. The apparent denaturing temperatures of T145LG and T145TG were 85 ± 1°C and 86 ±1°C respectively, almost the same as that of WT (85 ± 1°C). This suggests that the stabilities of T145LG and T145TG are almost the same as that of WT.

Activity of TLN variants at various concentrations of Zn^{2+} and of Co^{2+} – The FAGLA hydrolysis activities of WT, T145LG, and T145TG at various concentrations of Zn^{2+} and of Co^{2+} were examined (Fig. 7). In WT, the k_{cat}/K_m value decreased with increasing concentrations of Zn^{2+} and reached 40% at 500 μM, and increased with increasing concentrations of Co^{2+} and reached 400% at 1 mM, which coincided with previous results (*65, 66, 80*). T145LG and T145TG did not exhibit activity in all test

conditions (0–500 μM $ZnCl_2$ or 0–2 mM $CoCl_2$).

Discussion

Differences in effects of the conversion of the zinc-binding sequence on catalytic activity between TLN and DPP III – In this study, conversion of the zinc-binding motif sequence of TLN, $H^{142}ELTH^{146}$, to that of DPP III, $H^{142}ELLGH^{146}$ or $H^{142}ELTGH^{146}$, eliminated catalytic activity. T145LG and T145TG did not exhibit activity even in the presence of elevated concentrations of Zn^{2+} or Co^{2+}. This is in contrast to results reported previously, that conversion of the zinc-binding motif sequence of DPP III, $H^{450}ELLGH^{455}$, to that of a majority of zinc metalloproteinases, including TLN, $H^{450}ELGH^{455}$, did not affect catalytic activity (*81*), indicating a difference in the effects of conversion of the zinc-binding sequence on catalytic activity between TLN and DPP III. A difference was also reported as to the effects of replacement of metal ions. The replacement of active-site Zn^{2+} with Cu^{2+} or Ni^{2+} in TLN eliminated catalytic activity (*66, 65, 78–80*) while that in DPP III did not eliminate it (*77*).

Fukasawa *et al.* (*86*) and Hirose *et al.* (*87*) pointed out that the unique characteristics of DPP III could be ascribed to the flexibility and hydrogen bonding network in its active site as per the following results: (i) Crystallographic analysis of yeast DPP III has indicated that the turn of the α-helix that contains $H^{450}ELLGH^{455}$ is widened, suggesting that this enables both His450 and His455 to coordinate to active-site Zn^{2+} (*88*) (ii) A three-dimensional modeling analysis of rat DPP III indicated that Glu512 and Glu507 stabilize the coordination of His450 and His455 respectively to active-site Zn^{2+} (*86*). Electron paramagnetic analysis of wild-type rat DPP III in which Zn^{2+} was replaced with Cu^{2+} indicated Glu451, one of the residues in the zinc-binding motif, critical for catalytic activity, can approach the water molecule, however in the same Cu^{2+}-containing DPP III variant in which Leu453 was deleted, the Glu451 cannot approach it, suggesting that Glu451 of wild-type DPP III can work as a general base, while that of the variant cannot work as a general base (*87*).

Although zinc contents of the TLN variants were not measured, the results presented here suggest that the active site of TLN does not have the flexibility in DPP III: (i) In the modeled structure of T145TG, the side-chains of His142 and His146 are rotated and might be unable to chelate the active-site Zn^{2+} (Fig. 1). (ii) V140A was active, but V140A/T145LG and V140A/T145TG were inactive, suggesting that Val140→Ala does not lead to a widening of the turn of α-helix Val139-Thr149. (iii) T80S, T80S/T145LG, and T80S/T145TG were inactive, suggesting that Thr80→Ser disrupts the active-site geometry required for catalytic activity. Similar results have been reported for other zinc-metalloproteinases with zinc-binding motif HEXXH, *Bacteroides fragilis* toxin (*89*), or rat aminopeptidase B (*90*) that all single mutations in the zinc-binding motif sequence eliminated activity.

Effects of conversion of the zinc-binding sequence of TLN to that of DPP III on the expression and stability of TLN – Our initial attempt to produce TLN variants with the HEXXXH motif by expressing the pre-proenzyme in *E. coli* was unsuccessful. Analysis by SDS-PAGE did not reveal the TLN variants in the culture supernatants or inside the cells. This can be explained by the fact that the expression system we used required autocatalytic cleavage of the peptide bond linking the pro and mature sequences yet the variants with the HEXXXH motif lacked activity. We think that the pre-proTLN did not fold properly and was degraded by other cellular proteases. In this study, this problem was circumvented by co-expressing the mature and pro domains separately. This is in contrast with the results for *B. fragilis* toxin (*89*) and rat aminopeptidase B (*90*), in which inactive variant enzymes with a single amino acid mutation at the zinc-binding motif sequence were successfully produced in *E. coli* cells by expressing the pre-proenzyme. This is because they were processed by cellular proteinases.

In this study, similar amounts of purified preparations of WT, T145LG, and T145TG were obtained from transformed *E. coli* cells (Fig. 5A). They exhibited the same CD spectra at far and near UV at 25°C (Fig. 5B and C). Their apparent denaturing temperatures, based on the ellipticity at 222 nm, were almost the same as that of WT

(Fig. 6). Taken together, our results suggest that conversion of the HEXXH motif to HEXXXH does not noticeably affect the expression or stability of TLN.

The TLN variants with the HEXXXH motif bound to a substrate analog Gly-D-Phe (Fig. 4). Resins containing Gly-D-Phe, D-phenylalanine (D-Phe), or D-leucine (D-Leu) are routinely used in affinity purification of TLN (*91, 92*). They are based on the finding that TLN catalyzes specifically the hydrolysis of peptide bonds with bulky hydrophobic amino acid residues such as Phe or Leu at P1′ position (*16*). In this study, all the TLN variants bound to Gly-D-Phe (Fig. 4). Although there is no direct evidence that TLN variants with the HEXXXH motif bind to substrates of TLN such as FAGLA and ZDFM, our results suggest that conversion of the HEXXH motif to HEXXXH does not materially affect the geometry of the site required for substrate binding. A comparison of the active-site structure of WT (Fig. 1A), determined by crystallographic analysis, to that of T145TG (Fig. 1B), modeled using WT as template, indicated that these structures are similar except for the presence or absence of active-site Zn^{2+} and the position of the side-chain of Glu166. We think that the results presented here corroborate the credibility of the modeled structure of T145TG (Fig. 1B).

In conclusion, conversion of the zinc-binding motif sequence of TLN, HEXXH, to that of DPP III, HEXXXH, eliminates TLN activity. The HEXXH zinc-binding motif sequence appears critical for the catalytic activity of TLN, but not essential for proper folding or stability. To achieve a detailed understanding of the effects of the conversion of HEXXH to HEXXXH on the structure of TLN, further investigation, including crystallographic structural analysis and electron spin resonance analysis, might be helpful.

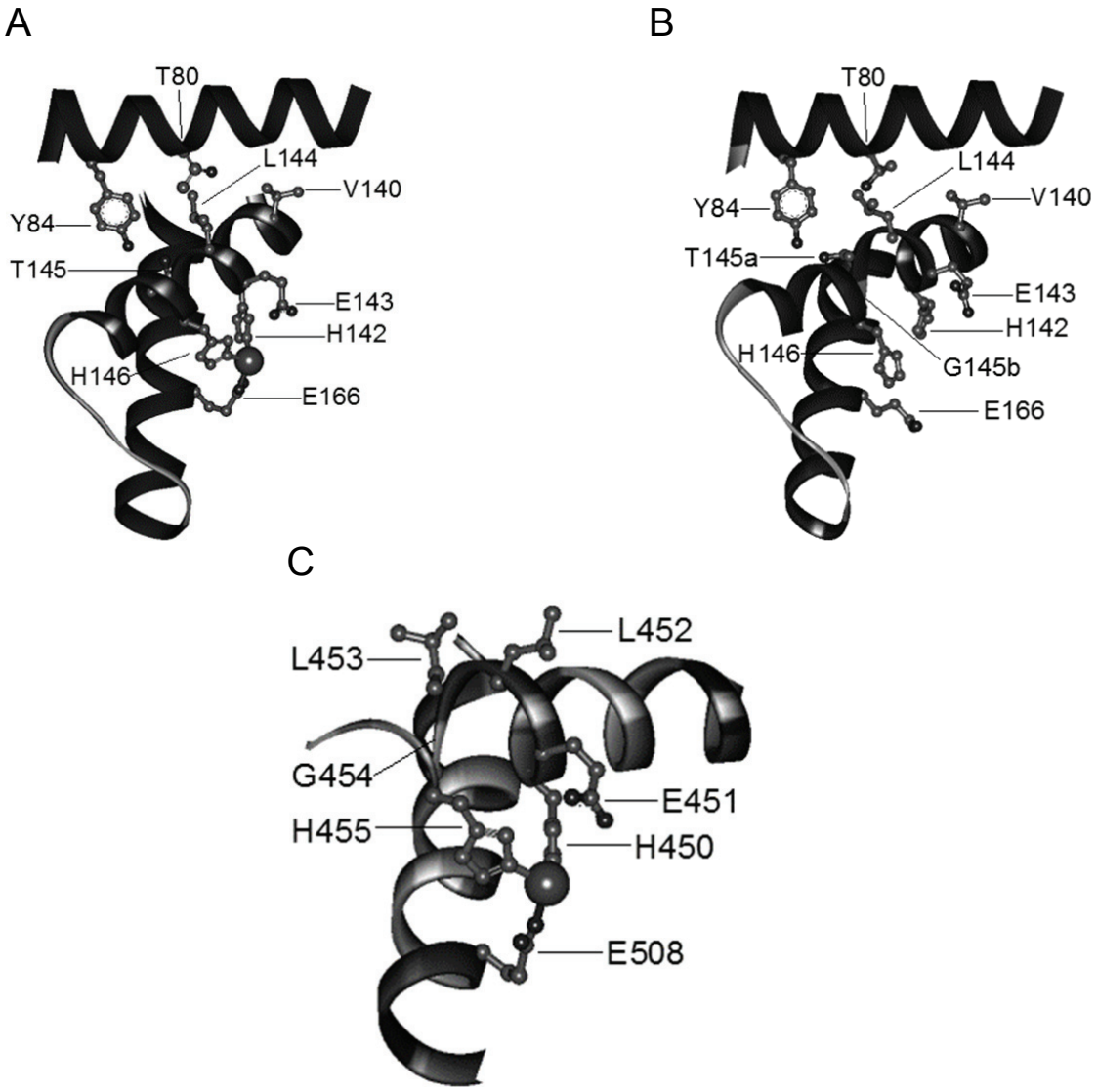

Fig. 1. Close-up view of the active sites of TLN and DPP III. (A) WT. The structure is based on PDB code 8TLN. (B) TLN variant T145TG. The 3D structural model was generated by the I-TASSER threading algorithm using WT as template. The overall protein structure (ribbon model), Thr80, Tyr84, Val140, His142, Glu143, Leu144, Thr145, Thr145a, Gly145b, His146, Glu166 (ball and stick), and the zinc ion (sphere) are shown. (C) DPP III. The structure is based on PDB code 3FVY. The overall protein structure (ribbon model), His450, Glu451, Leu452, Leu453, Gly454, His455, Glu508 (ball and stick), and the zinc ion (sphere) are shown.

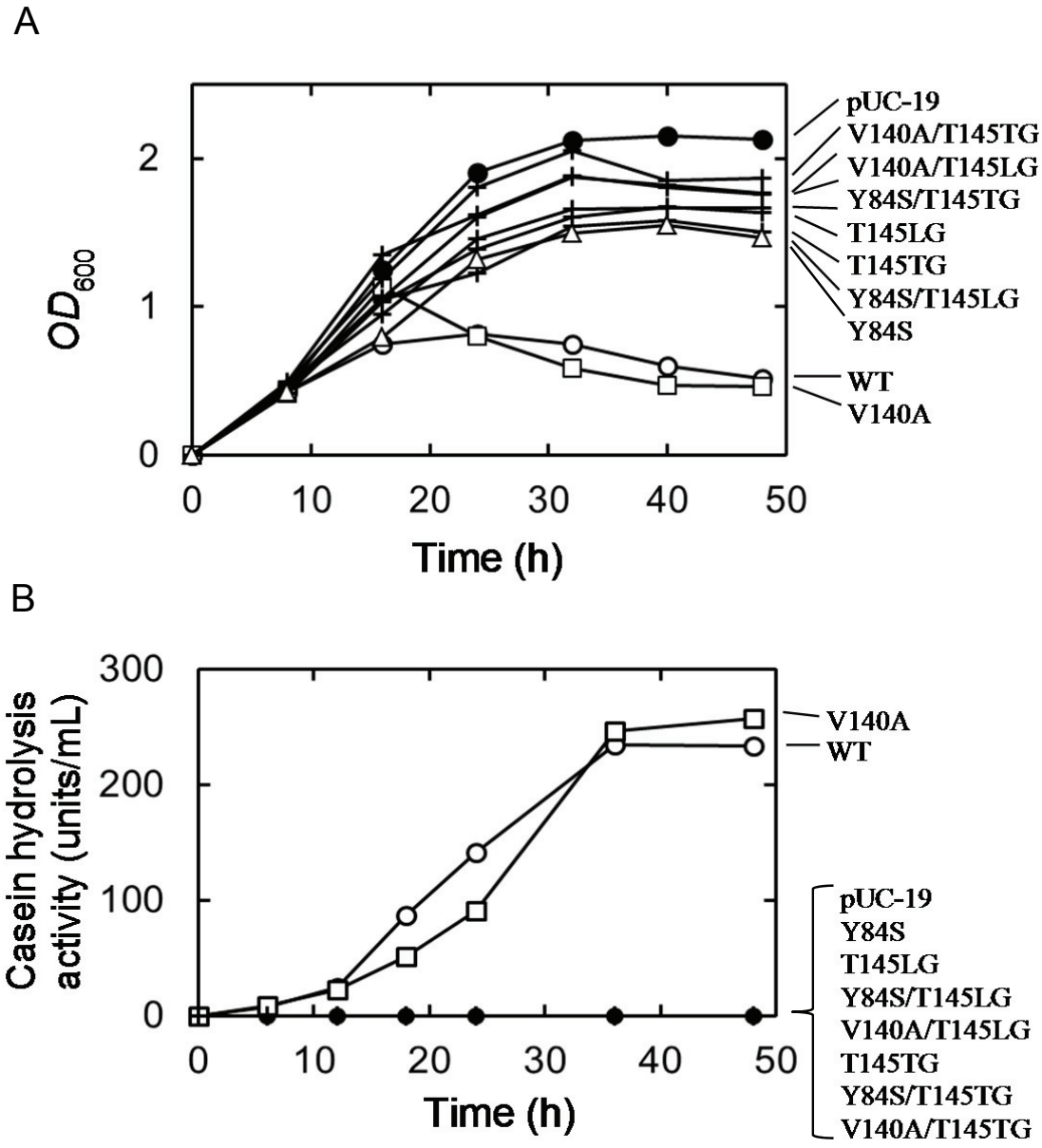

Fig. 2. Culturing of *E. coli*. (A) Cell densities. (B) Casein hydrolysis activities. OD_{600} of culture (A) and casein hydrolysis activities of the culture supernatants (B) of *E. coli* cells transformed with pUC19 (●) or the expression plasmids for WT (○), Y84S (Δ), V140A (□), and the other six variants (T145LG, Y84S/T145LG, V140A/T145LG, T145TG, Y84S/T145TG, and V140A/T145TG) (+) are plotted against time. In Fig. 2B, the points of the six variants overlap with those of pUC19, and are invisible. 0 h means start of flask-shake culture.

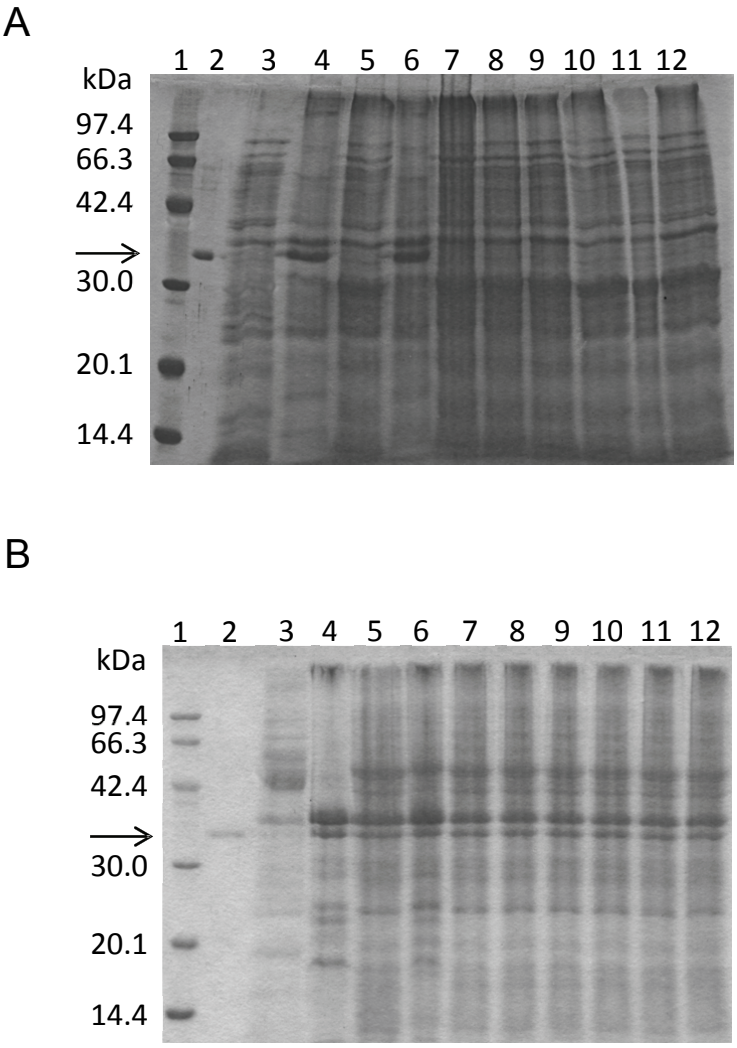

Fig. 3. Expression of TLN variants. Coomassie Brilliant Blue-stained 12.5% SDS-PAGE are shown. (A, B) The marker proteins (lane 1), native TLN purified from *B. thermoproteolyticus* (lane 2), and the culture supernatants (A), or the soluble fractions (B) of the *E. coli* cells transformed with pUC-19 (lane 3), and the expression plasmids for WT (lane 4), Y84S (lane 5), V140A (lane 6), 145LG (lane 7), Y84S/T145LG (lane 8), V140A/T145LG (lane 9), T145TG (lane 10), Y84S/T145TG (lane 11), and V140A/T145TG (lane 12). Arrow indicates the position of mature TLN band.

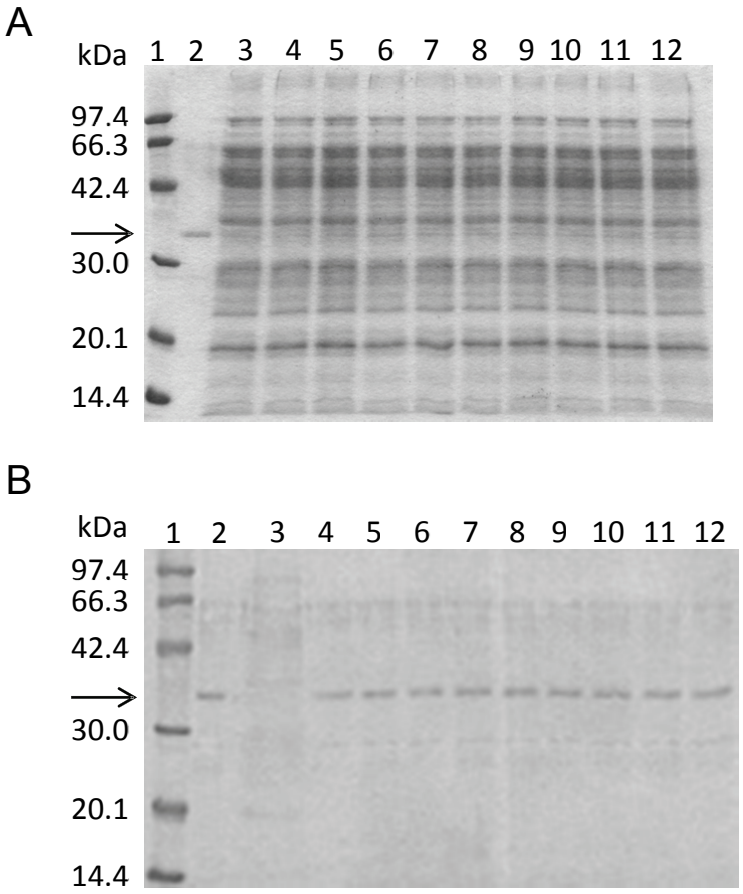

Fig. 4. Gly-D-Phe-binding abilities of TLN variants. Coomassie Brilliant Blue-stained 12.5% SDS-PAGE are shown. (A, B) The marker proteins (lane 1), native TLN purified from *B. thermoproteolyticus* (lane 2), the pass-through fractions (A) and the eluted fractions (B) of Gly-D-Phe column chromatography of the soluble fractions of *E. coli* cells transformed with pUC-19 (lane 3), and the expression plasmids for WT (lane 4), Y84S (lane 5), V140A (lane 6), T145LG (lane 7), Y84S/T145LG (lane 8), V140A/T145LG (lane 9), T145TG (lane 10), Y84S/T145TG (lane 11), and V140A/T145TG (lane 12) are shown. Arrow indicates the position of mature TLN band.

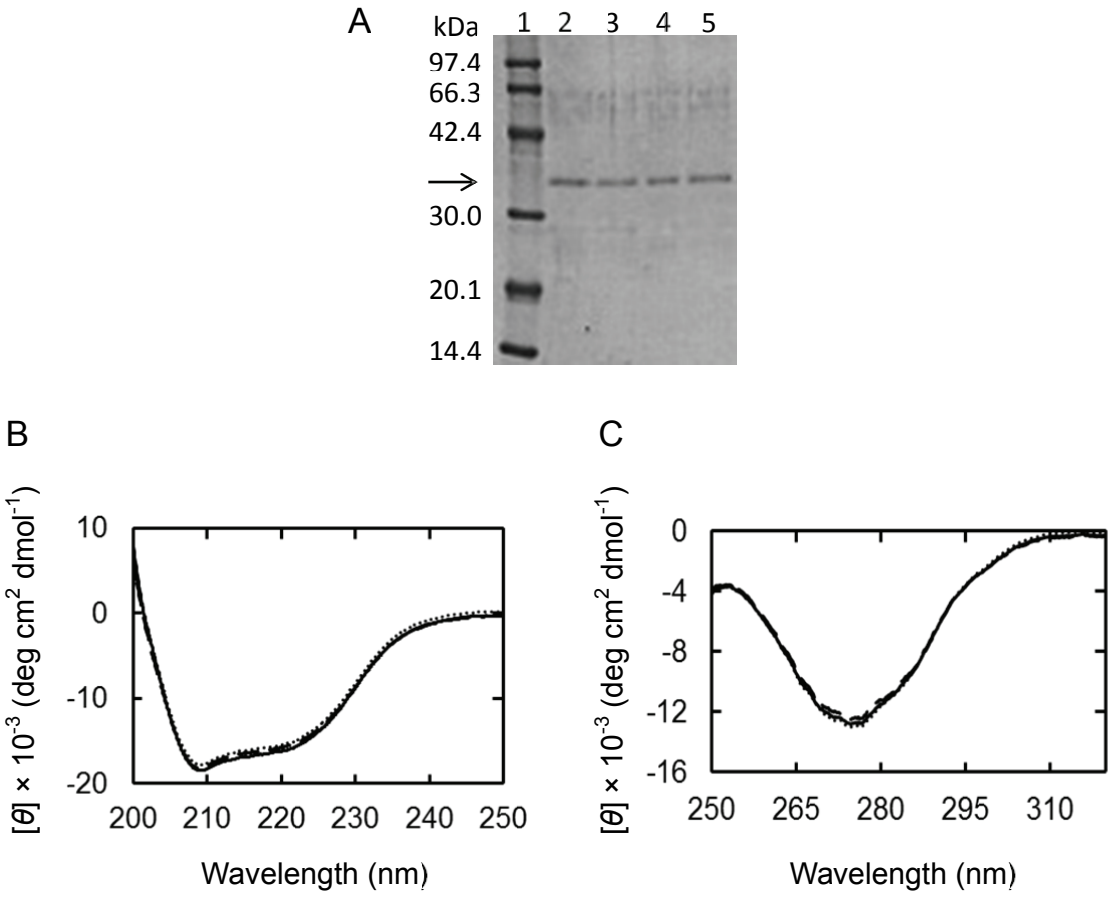

Fig. 5. Purification of TLN variants. (A) Coomassie Brilliant Blue-stained 12.5% SDS-PAGE are shown. The marker proteins (lane 1), native TLN purified from *B. thermoproteolyticus* (lane 2), WT (lane 3), T145LG (lane 4), and T145TG (lane 5). Arrow indicates the position of mature TLN band. (B, C) Far-UV (B) and near-UV (C) CD spectroscopy at 25°C of WT (——), T145LG (- - - -), and T145TG (·····).

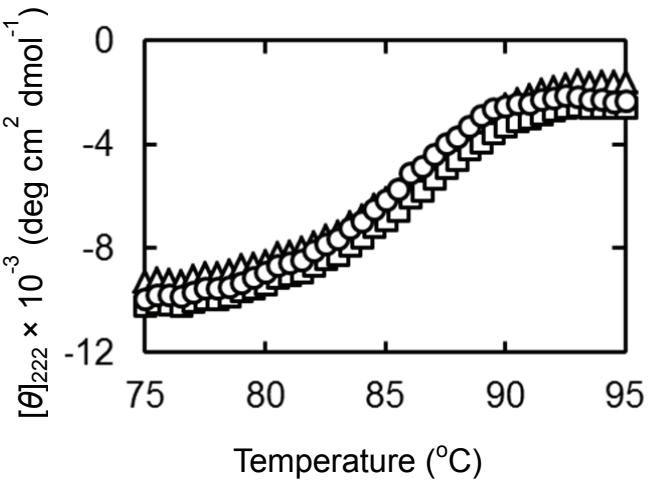

Fig. 6. Thermal denaturation of TLN variants. The θ_{222} for WT, T145LG, and T145TG were monitored from 75 to 95ºC at 0.5ºC/min. Markers: WT (○), T145LG (Δ), and T145TG (□).

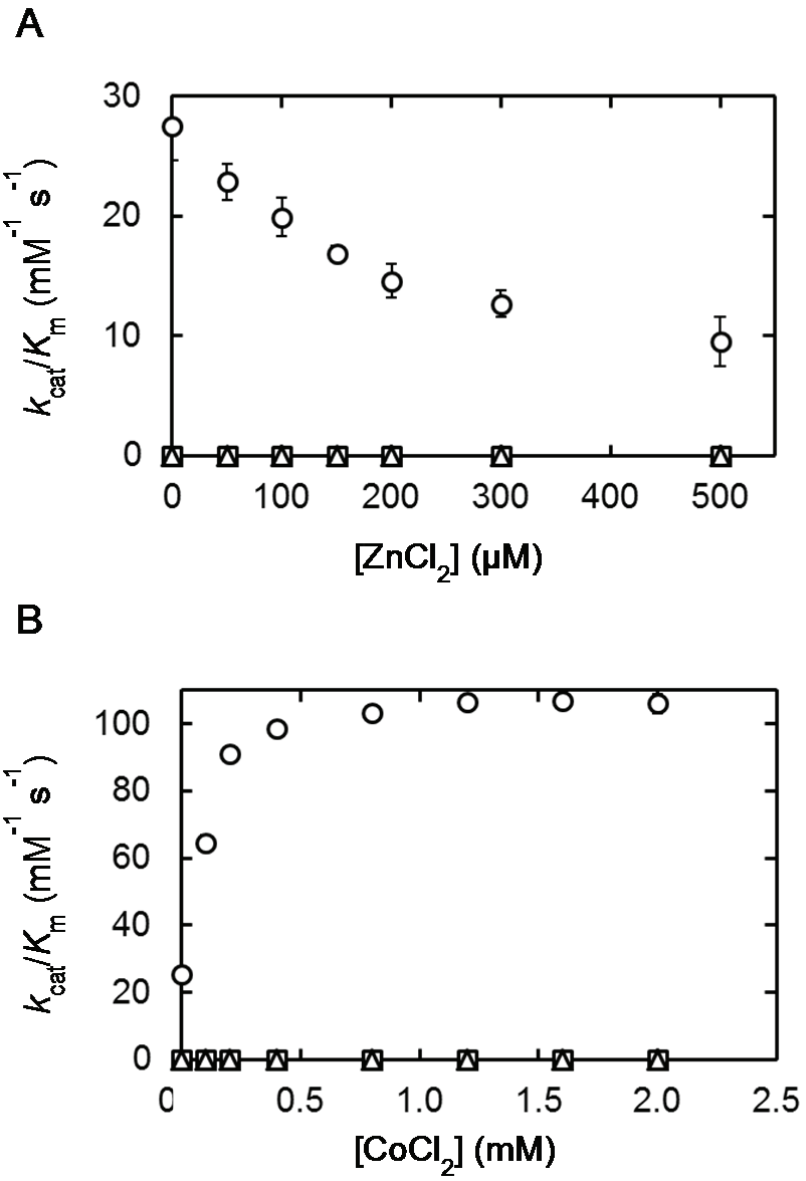

Fig. 7. Effects of zinc and cobalt ions on the activities of TLN variants. TLN (2 μM) was incubated with $ZnCl_2$ (0–500 μM) (A) or $CoCl_2$ (0–2 mM) (B) for 1 h on ice. Then the FAGLA hydrolysis reaction was carried out with concentrations of TLN, FAGLA, and $ZnCl_2$ or $CoCl_2$ at 0.1 μM, 400 μM, and 0–500 μM or 0–2 mM respectively. Markers: WT (○), T145LG (Δ), and T145TG (□).

Summary

Chapter 1

In the N-terminal domain of TLN, two polypeptide strands, Asn112-Trp115 and Ser118-Tyr122, are connected by a short loop, Asn116-Gly117, to form an anti-parallel β-sheet. The Asn112-Trp115 strand is located in the active site, while the Ser118-Tyr122 strand and the Asn116-Gly117 loop are located outside the active site. In this study, we explored the catalytic role of Gly117 by site-directed mutagenesis. Four variants, G117D, G117E, G117K, and G117R, were produced by co-expressing in *E. coli* the mature and pro domains as independent polypeptides. The production levels were in the order G117E > wild type > G117K, G117R > G117D. G117A was hardly produced. This result was in contrast to a previous study in which all 72 active-site TLN variants were produced at a similar level whether or not they retained activity. G117E exhibited lower activity in the hydrolysis of FAGLA and higher activity in the hydrolysis of ZDFM than WT. G117K and G117R exhibited considerably reduced activities. This suggests that Gly117 plays an important role in the activity and stability of TLN, presumably by affecting the geometries of the Asn112-Trp115 and Ser118-Tyr122 strands.

Chapter 2

In the N-terminal domain of TLN, two anti-parallel β-strands, Asn112-Trp115 and Ser118-Tyr122 are connected by an Asn116-Gly117 turn to form a β-hairpin structure. In this study, we examined the role of Asn116 in the activity and stability of TLN by site-directed mutagenesis. Of the 19 Asn116 variants, four (N116A, N116D, N116T, and N116Q) were produced in *E. coli*, by co-expressing the mature and pro domains

separately, while the other 15 could not be produced. In the hydrolysis of FAGLA at 25°C, the intrinsic k_{cat}/K_m value of N116D was 320% of that of the WT, and in the hydrolysis of ZDFM at pH 7.5 at 25°C, the k_{cat}/K_m value of N116D was 140% of that of WT, indicating that N116D exhibited higher activity than WT. N116Q exhibited similar activity as WT, and N116A and N116T exhibited reduced activities. The k_{obs} values at 80°C were in the order N116A, N116D, N116T > N116Q > WT at all $CaCl_2$ concentrations examined (1–100 mM), indicating that all variants exhibited reduced stabilities. These results suggest that Asn116 plays an important role in the activity and stability of TLN presumably by stabilizing this β-hairpin structure.

Chapter 3

Neutral salts activate and stabilize TLN. In this study, we examined the effects of two activating mutations, Asn116→Asp and Asp150→Glu, on NaCl-induced activation and stabilization of TLN. In the hydrolysis of FAGLA, the relative activities (ratios of k_{cat}/K_m, at x M NaCl to that at 0 M NaCl) at 0.5–4.0 M NaCl of D150E and N116D/D150E were lower than those of WT and N116D, respectively. In the thermal inactivation at 70ºC, the relative stabilities (ratios of the k_{obs} at 0 M NaCl to that at x M NaCl) at 0.5–4.0 M NaCl of D150E and N116D/D150E were lower than those of WT and N116D, respectively. These results indicate that unlike Asn116→Asp, Asp150→Glu reduced the NaCl-induced activation and stabilization, suggesting the binding of ions with certain residue(s) of TLN is involved in the activation and stabilization.

Chapter 4

Most zinc metalloproteinases have the consensus zinc-binding motif sequence HEXXH, in which two histidine residues chelate a catalytic zinc ion. The zinc-binding

motif sequence of TLN, $H^{142}ELTH^{146}$, belongs to this motif sequence, while that of DPP III, $H^{450}ELLGH^{455}$, belongs to the motif sequence HEXXXH. In this study, we examined effects of conversion of HEXXH to HEXXXH in TLN on its activity and stability. TLN variants bearing $H^{142}ELLGH^{146}$ or $H^{142}ELTGH^{146}$ (designated T145LG and T145TG, respectively) were constructed by site-directed mutagenesis and were produced in *E. coli* cells by co-expressing the mature and pro domains separately. They did not exhibit hydrolyzing activity for casein or FAGLA, but exhibited binding ability to a substrate analog Gly-D-Phe. The apparent denaturing temperatures based on ellipticity at 222 nm of T145LG and T145TG were 85 ± 1°C and 86 ± 1°C, respectively, almost the same as that of WT (85 ± 1°C). These results indicate that conversion of HEXXH to HEXXXH abolishes TLN activity, but does not affect its binding ability to Gly-D-Phe or its stability. Our results are in contrast to ones reported previously, that DPP III variants bearing $H^{450}ELGH^{455}$ exhibit activity.

References

1. Endo, S. (1962) Studies on protease produced by thermophilic bacteria. *J. Ferment. Technol.* **40**, 346–353
2. van den Burg, B. and Eijsink, V.G. (2004) Thermolysin in *Handbook of Proteolytic Enzymes,* 2nd ed. (Barrett, J.A., Rawlings, N.D., and Woessner, J.F. eds.) Vol. 1, pp. 374–387, Elsevier, Amsterdam, The Netherlands
3. Inouye, K. (2003) Thermolysin in *Handbook of Food Enzymology* (Whitaker, J.R., Voragen, A.G.J., and Wong, D.W.S. eds.) pp. 1019–1028, Marcel Dekker, New York
4. Latt, S.A., Holmquist, B., and Vallee, B.L. (1969) Thermolysin: a zinc metalloenzyme. *Biochem. Biophys. Res. Commun.* **37**, 333–339
5. Feder, J., Garrett, L.R., and Wildi, B.S. (1971) Studies on the role of calcium in thermolysin. *Biochemistry* **10**, 4552–4556
6. Tajima, M., Urabe, I., Yutani, K., and Okada, H. (1976) Role of calcium ions in the thermostability of thermolysin and *Bacillus subtilis* var. *amylosacchariticus* neutral protease. *Eur. J. Biochem.* **64**, 243–247
7. Titani, K., Hermodson, M.A., Ericsson, L.H., Walsh, K.A., and Neurath, H. (1972) Amino-acid sequence of thermolysin. *Nature* **238**, 35–37
8. O'Donohue, M.J., Roques, B.P., and Beaumont, A. (1994) Cloning and expression in *Bacillus subtilis* of the npr gene from *Bacillus thermoproteolyticus* Rokko coding for the thermostable metalloprotease thermolysin. *Biochem. J.* **300**, 599–603
9. Hangauer, D.G., Monzingo, A.F., and Matthews, B.W. (1984) An interactive computer graphics study of thermolysin-catalyzed peptide cleavage and inhibition by *N*-carboxymethyl dipeptides. *Biochemistry* **23**, 5730–5741
10. Holmes, M.A. and Matthews, B.W. (1982) Structure of thermolysin refined at 1.6 Å resolution. *J. Mol. Biol.* **160**, 623–639
11. Mock, W.L. and Aksamawati, M. (1994) Binding of thermolysin of

phenolate-containing inhibitors necessitates a reversed mechanism of catalysis. *Biochem. J.* **302**, 57–68

12. Kusano, M., Yasukawa, K., and Inouye, K. (2009) Insights into the catalytic roles of the polypeptide regions in the active site of thermolysin and generation of thermolysin variants with high activity and stability. *J. Biochem.* **145**, 103–113
13. Lenart, A., Dudkiewicz, M., Grynberg, M., and Pawłowski, K. (2013) CLCAs - A family of metalloproteases of intriguing phylogenetic distribution and with cases of substituted catalytic sites. *PLoS ONE 8(5): e62272. doi:10.1371/journal.pone.0062272*
14. Fukasawa, K.M, Hata, T., Ono, Y., and Hirose, J. (2011) Metal preferences of zinc-binding motif on metalloproteases. *J. Amino Acids* **2011**, 574816.
15. Gomis-Ruth, F.X., Grams, F., Yiallouros, I., Nar, H., Küsthardt, U., Zwilling, R., Bode, W., and Stöcker, W. (1994) Crystal structures, spectroscopic features, and catalytic properties of cobalt(II), copper(II), nickel(II), and mercury(II) derivatives of the zinc endopeptidase astacin. A correlation of structure and proteolytic activity. *J. Biol. Chem.* **269**, 17111–17117
16. Morihara, K. and Tsuzuki, H. (1970) Thermolysin: kinetic study with oligopeptides. *Eur. J. Biochem.* **15**, 374–380
17. Inouye, K., Lee, S-B., and Tonomura, B. (1996) Effect of amino acid residues at the cleavable site of substrates on the remarkable activation of thermolysin by salts. *Biochem. J.* **315**, 133–138
18. Inouye, K. (1992) Effects of salts on thermolysin: activation of hydrolysis and synthesis of *N*-carbobenzoxy-L-aspartyl-L-phenylalanine methyl ester, and a unique change in the absorption spectrum of thermolysin. *J. Biochem.* **112**, 335–340
19. Oyama, K., Kihara, K., and Nonaka, Y. (1981) On the mechanism of the action of thermolysin: kinetic study of the thermolysin-catalyzed condensation reaction of *N*-benzyloxycarbonyl-L-aspartic acid with L-phenylalanine methyl ester. *J. Chem. Soc. Perkin II* 356–360
20. Inouye, K., Kuzuya, K., and Tonomura, B. (1988) Sodium chloride enhances

markedly the thermal stability of thermolysin as well as its catalytic activity. *Biochim. Biophys. Acta* **1388**, 209–214

21. Inouye, K., Lee, S-B., Nambu, K., and Tonomura, B. (1997) Effects of pH, temperature, and alcohols on the remarkable activation of thermolysin by salts. *J. Biochem.* **122**, 358–364
22. Oneda, H., Muta, Y., and Inouye, K. (2004) Substrate-dependent activation of thermolysin by salt. *Biosci. Biotechnol. Biochem.* **68**, 1811–1813
23. Inouye, K., Kuzuya, K., and Tonomura, B. (1998) Effect of salts on the solubility of thermolysin: a remarkable increase in the solubility as well as the activity by the addition of salts without aggregation or dispersion of thermolysin. *J. Biochem.* **123**, 847–852
24. Toma, S., Campagnoli, S., de Gregoriis, E., Gianna, R., Margarit, I., Zamai, M., and Grandi, G. (1989) Effect of Glu-143 and His-231 substitutions on the catalytic activity and secretion of *Bacillus subtilis* neutral protease. *Protein Eng.* **2**, 359–364
25. Inouye, K., Mazda, N., and Kubo, M. (1998) Need for aromatic residue at position 115 for proteolytic activity found by site-directed mutagenesis of tryptophan 115 in thermolysin. *Biosci. Biotechnol. Biochem.* **62**, 798–800
26. Hanzawa, S. and Kidokoro, S. (1999) Thermolysin in *Encyclopedia of Bioprocess Technology*: *Fermentation, Biocatalysis, and Bioseparation* (Flickinger, M.C and Drew S.W., eds.) pp. 2527–2535, John Wiley & Sons, New York
27. Matsumiya, Y., Nishikawa, K., Aoshima, H., Inouye, K., and Kubo, M. (2004) Analysis of autodegradation sites of thermolysin and enhancement of its thermostability by modifying Leu155 at an autodegradation site. *J. Biochem.* **135**, 547–553
28. Matsumiya, Y., Nishikawa, K., Inouye, K., and Kubo, M. (2005) Mutational effect for stability in a conserved region of thermolysin. *Lett. Appl. Microbiol.* **40**, 329–334
29. Kusano, M., Yasukawa, K., Hashida, Y., and Inouye, K. (2006) Engineering of the pH-dependence of thermolysin activity as examined by site-directed mutagenesis

of Asn112 located at the active site of thermolysin. *J. Biochem*. **139**, 1017–1023

30. Tatsumi, C., Hashida, Y., Yasukawa, K., and Inouye, K. (2007) Effects of site-directed mutagenesis of the surface residues Gln128 and Gln225 of thermolysin on its catalytic activity. *J. Biochem.* **141**, 835–842
31. Yasukawa, K. and Inouye, K. (2007) Improving the activity and stability of thermolysin by site-directed mutagenesis. *Biochim. Biophys. Acta* **1774**, 1281–1288
32. Kusano, M., Yasukawa, K., and Inouye, K. (2010) Effects of the mutational combinations on the activity and stability of thermolysin. *J. Biotechnol.* **147**, 7–16
33. Feder, J. (1968) A spectrophotometric assay for neutral protease. *Biochem. Biophys. Res. Commun.* **32**, 326–332
34. Yasukawa, K., Kusano, M., and Inouye, K. (2007) A new method for the extracellular production of recombinant thermolysin by co-expressing the mature sequence and pro-sequence in *Escherichia coli*. *Protein Eng. Des. Sel.* **20**, 375–383
35. Inouye, K., Minoda, M., Takita, T., Sakurama, H., Hashida, Y., Kusano, M., and Yasukawa, K. (2006) Extracellular production of recombinant thermolysin expressed in *Escherichia coli*, and its purification and enzymatic characterization. *Protein Expr. Purif.* **46**, 248–255
36. Yasukawa, K., Kusano, M., Nakamura, K., and Inouye, K. (2006) Characterization of Gly-D-Phe, Gly-L-Leu, and D-Phe as affinity ligands to thermolysin. *Protein Expr. Purif.* **46**, 332–336
37. Laemmli, U.K. (1970) Cleavage of structural proteins during the assembly of the head of bacteriophage T4. *Nature* **227**, 680–685
38. Sakoda, M. and Hiromi, K. (1976) Determination of the best-fit values of kinetic parameters of the Michaelis-Menten equation by the method of least squares with the Taylor expansion. *J. Biochem.* **80**, 547–555
39. Takita, T., Aono, T., Sakurama, H., Itoh, T., Wada, T., Minoda, M., Yasukawa, K., and Inouye, K. (2008) Effects of introducing negative charges into the molecular surface of thermolysin by site-directed mutagenesis on its activity and stability.

Biochim. Biophys. Acta **1784**, 481–488

40. Tronrud, D.E., Holden, H.M., and Matthews, B.W. (1987) Structures of two thermolysin-inhibitor complexes that differ by a single hydrogen bond. *Science* **235**, 571–574
41. Eijsink, V.G., van den Burg, B., Vriend, G., Berendsen, H.J., and Venema, G. (1991) Thermostability of *Bacillus Subtilis* neutral protease. *Biochem. Int.* **24**, 517–525
42. Mansfeld, J. and Ulbrich-Hofmann, R. (2006) The stability of engineered thermostable neutral proteases from *Bacillus stearothermophilus* in organic solvents and detergents. *Biotechnol. Bioeng.* **97**, 672–679
43. Durrschmidt, P., Mansfeld, J., and Ulbrich-Hofmann, R. (2010) Refolding of the non-specific neutral protease from *Bacillus stearothermophilus* proceeds via an autoproteolytically sensitive intermediate. *Biophys. Chem.* **147**, 66–73
44. Taylor, W.R. (1986) The classification of amino acid conservation. *J. Theor. Biol.* **119**, 205–218
45. Kyrieleis, O.J., Goettig, P., Kiefersauer, R., Huber, R., and Brandstetter, H. (2005) Crystal structures of the tricorn interacting factor F3 from *Thermoplasma acidophilum*, a zinc aminopeptidase in three different conformations. *J. Mol. Biol.* **349**, 787–800
46. Addlagatta, A., Gay, L., and Mathews, B.W. (2006) Structure of aminopeptidase N from *Escherichia coli* suggests a compartmentalized, gated active site. *Proc. Natl. Acad. Sci. USA* **103**, 13339–13344
47. Ito, K., Nakajima, Y., Onohara, Y., Takeo, M., Nakashima, K., Matsubara, F., Ito, T., and Yoshimoto, T. (2006) Crystal structure of aminopeptidase N (proteobacteria alanyl aminopeptidase) from *Escherichia coli* and conformational change of methionine 260 involved in substrate recognition. *J. Biol. Chem.* **281**, 33664–33676
48. Schechter, I. and Berger, A. (1967) On the size of the active site in proteases. I. Papain. *Biochem. Biophys. Res. Commun.* **27**, 157–162
49. Kawasaki, Y., Yasukawa, K., and Inouye, K. (2013) Effects of site-directed

mutagenesis in the N-terminal domain of thermolysin on its stabilization. *J. Biochem.* **153**, 85–92

50. Kelly, S.M, Jess, T.J., and Price, N.C. (2005) How to study proteins by circular dichroism. *Biochim. Biophys. Acta* **1751**, 119–139
51. Sibanda, B.L., Blundell, T.L., and Thornton, J.M. (1989) Conformation of β-hairpins in protein structure. A systematic classification with applications to modelling by homology, electron density fitting and protein engineering. *J. Mol. Biol.* **206**, 759–777
52. Santiveri, C.M. and Jiménez, M.A. (2010) Tryptophan residues: scarce in proteins but strong stabilizers of β-hairpin peptides. *Peptide Sci.* **94**, 779–790
53. Hwang, S. and Hilty, C. (2012) Folding of a tryptophan zipper peptide investigated on the basis of the nuclear Overhauser effect and thermal denaturation. *J. Phys. Chem. B.* **115**, 15355–15361
54. Wu, L., McElheny, D., Setnicka, V., Hilario, J., and Keiderling, T.A. (2012) Role of different β-turns in β-hairpin conformation and stability studies by optical spectroscopy. *Proteins* **80**, 44–60
55. Shoichet, B.K., Baase, W.A., Kuroki, R., and Matthews, B.W. (1995) A relationship between protein stability and protein function. *Proc. Natl. Acad. Sci. USA.* **92**, 452–456
56. Lee, S., Oneda, H., Minoda, M., Tanaka, A., and Inouye, K. (2006) Comparison of starch hydrolysis activity and thermal stability of two *Bacillus licheniformis* α-amylase and insights into engineering α-amylase variants active under acidic conditions. *J. Biochem.* **139**, 997–1005
57. Lister, S.A., Wetmore, D.R., Roche, R.S., and Codding, P.W. (1996) E144S active-site mutant of the *Bacillus cereus* thermolysin-like neutral protease at 2.8 Å resolution. *Acta Crystallogr. D Biol. Crystallogr.* **52**, 543–550
58. Thayer, M.M., Flaherty, K.M., and KcKay, D.B. (1991) Three-dimensional structure of the elastase of *Pseudomonas aeruginosa* at 1.5-Å resolution. *J. Biol. Chem.* **266**, 2864–2871
59. Gao, X., Wang, J., Yu, D.Q., Bian, F., Xie, B.B., Chen, X.L., Zhou, B.C., Lai, L.H.,

Wang, Z.X., Wu, J.W., and Zhang, Y.Z. (2010) Structural basis for the autoprocessing of zinc metalloproteases in the thermolysin family. *Proc. Natl. Acad. Sci. USA* **107**, 17569–17574

60. Demidyuk, I.V., Gromova, T.Y., Polyakov, K.M., Melik-Adamyan, W.R., Kuranova, I.P., and Kostrov, S.V. (2010) Crystal structure of the protealysin precursor: insights into propeptide function. *J. Biol. Chem.* **285**, 2003–2013
61. Natesh, R., Schwager, S.L., Sturrock, E.D., and Acharya, K.R. (2003) Crystal structure of the human angiotensin-converting enzyme-lisinopril complex. *Nature* **421**, 551–554
62. Wondrak, E.M., Louis, J.M., and Oroszlan, S. (1991) The effect of salt on the Michaelis Menten constant of the HIV-1 protease correlates with the Hofmeister series. *FEBS Lett.* **280**, 344–346
63. Porter, D.J.T., Hanlon, M.H., Carter, L.H. III, Danger, D.P., and Furfine, E.S. (2001) Effectors of HIV-1 protease peptidolytic activity. *Biochemistry* **40**, 11131–11139
64. Tronrud, D.E., Monzingo, A.F., and Matthews, B.W. (1986) Crystallographic structural analysis of phosphoramidates as inhibitors and transition-state analogs of thermolysin. *Eur. J. Biochem.* **157**, 261–268
65. Hashida, Y. and Inouye, K. (2007) Kinetic analysis of the activation-and-inhibition dual effects of cobalt ion on thermolysin activity. *J. Biochem.* **141**, 843–853
66. Hashida, Y. and Inouye, K. (2007) Molecular mechanism of the inhibitory effect of cobalt ion on thermolysin activity and the suppressive effect of calcium ion on the cobalt ion-dependent inactivation of thermolysin *J. Biochem.* **141**, 879–888
67. Inouye, K. (1994) [Halophilic enzymes]. *Seikagaku* (in Japanese) **66**, 446–450
68. Madern, D. and Ebel, C. (2007) Influence of an anion-binding site in the stabilization of halophilic malate dehydrogenase from *Haloarcula marismortui*. *Biochimie* **89**, 981–987
69. Arai, S., Yonezawa, Y., Okazaki, N., Matsumoto, F., Tamada, T., Tokunaga, H., Ishibashi, M., Blaber, M., Tokunaga, M., and Kuroki, R. (2012) A structural

mechanism for dimeric to tetrameric oligomer conversion in *Halomonas* sp. nucleoside diphosphate kinase. *Protein Sci.* **21**, 498–510

70. Rushworth, C.A., Guy, J.L., and Turner, A.J. (2008) Residues affecting the chloride regulation and substrate selectivity of the angiotensin-converting enzymes (ACE and ACE2) identified by site-directed mutagenesis. *FEBS J.* **275**, 6033–6042
71. Kamo, M., Inouye, K., Nagata, K., and Tanokura, M. (2005) Preliminary X-ray crystallographic analysis of thermolysin in the presence of 4 M NaCl. *Acta Cryst.* **D61**, 710–712
72. Ellis, S. and Nuenke, J.M. (1967) Dipeptidyl arylamidase III of the pituitary: purification and characterization. *J. Biol. Chem.* **242**, 4623–4629
73. Fukasawa, K., Fukasawa, K.M., Kanai, M., Fujii, S., Hirose, J., and Harada, M. (1998) Dipeptidyl peptidase III is a zinc metallo-exopeptidase: molecular cloning and expression. *Biochem. J.* **329**, 275–282
74. Ohkubo, I., Li, Y-H., Maeda, T., Yamamoto, Y., Yamane, T., Du, P-G., and Nishi, K. (2000) Molecular cloning and immunohistochemical localization of rat dipeptidyl peptidase III. *Forensic Sci. Int.* **113**, 147–151
75. Fukasawa, K., Fukasawa, K.M, Iwamoto, H., Hirose, J., and Harada, M. (1999) The HELLGH motif of rat liver dipeptidyl peptidase III is involved in zinc coordination and the catalytic activity of the enzyme. *Biochemistry* **38**, 8299–8303
76. Prajapati, S.C and Chauhan, S.S. (2011) Dipeptidyl peptidase III: a multifaceted oligopeptide N-end cutter. *FEBS J.* **278**, 3256–3276
77. Hirose, J., Iwamoto, H., Nagao, I., Enmyo, K., Sugao, H., Kanemitu, N., Ikeda, K., Takeda, M., Inoue, M., Ikeda, T., Matsuura, F., Fukasawa, K.M., and Fukasawa, K. (2001) Characterization of the metal-substituted dipeptidyl peptidase III (rat liver) *Biochemistry* **40**, 11860–11865
78. Holmquist, B. and Vallee, B.L. (1974) Metal substitutions and inhibition of thermolysin: spectra of the cobalt enzyme. *J. Biol. Chem.* **249**, 4601–4607
79. Holland, D.R., Hausrath, A.C., Juers, D., and Matthews, B.W. (1995) Structural analysis of zinc substitutions in the active site of thermolysin. *Protein Sci.* **4**,

1955–1965

80. Kuzuya, K. and Inouye, K. (2001) Effects of cobalt-substitution of the active zinc ion in thermolysin on its activity and active-site microenvironment. *J. Biochem.* **130**, 783–788

81. Hirose, J., Kamigakiuchi, H., Iwamoto, F.H., Nakai, M., Takenaka, M., Kataoka R., Sugahara, M., Yamamoto, S., and Fukasawa, K.M. (2004) The metal-binding motif of dipeptidyl peptidase III directly influences the enzyme activity in the copper derivative of dipeptidyl peptidase III. *Arch*. *Biochem*. *Biophys.* **431**, 1–8

82. Zhang, Y. (2008) I-TASSER server for protein 3D structure prediction. *BMC Bioinformatics* **9**, 40

83. Roy, A., Kucukural, A., and Zhang, Y. (2010) I-TASSER: a unified platform for automated protein structure and function prediction. *Nat. Protoc.* **5**, 725–738

84. Roy, A., Yang, J., and Zhang, Y. (2012) COFACTOR: An accurate comparative algorithm for structure-based protein function annotation. *Nucleic Acids Res.* **40**, W471–W477

85. Daly, T.K., Sutherland-Smith, A.J., and Penny, D. (2012) Beyond BLASTing: tertiary and quaternary structure analysis helps identify major vault proteins. *Genome Biol. Evol.* **5**, 217–232

86. Fukasawa, K.M., Hirose, J., Hata, T., and Ono, Y. (2010) In rat dipeptidyl peptidase III, His568 is essential for catalysis, and Glu507 or Glu512 stabilizes the coordination bond between His455 or His450 and zinc ion. *Biochim. Biophys. Acta* **1804**, 2063–2069

87. Hirose, J., Hata, T., Kawaoka, C., Ikeura, T., Kitahara, S., Horii, K., Tomida, H., Iwamoto, H., Ono Y., and Fukasawa, K.M (2012) Flexibility of the coordination geometry around the cupric ions in Cu(II)-rat dipeptidyl peptidase III is important for the expression of enzyme activity. *Arch. Biochem. Biophys.* **525**, 71–81

88. Baral, P.K., Jajćanin-Jozić, N., Deller, S., Macheroux, P., Abramić, M., and Gruber, K. (2008) The first structure of dipeptidyl-peptidase III provides insight into the catalytic mechanism and mode of substrate binding. *J. Biol. Chem.* **283**, 22316–22324

89. Franco, A.A., Buckwold, S.L., Shin, J.W., Ascon, M., and Sears, C.L. (2005) Mutation of the zinc-binding metalloprotease motif affects *Bacteroides fragilis* toxin activity but does not affect propeptide processing. *Infect. Immun.* **73**, 5273–5277

90. Viet-Laï, P., Cadel, M-S., Darmon, C.G., Hanquez, C., Beinfeld, M.C., Nicolas, P., Etchebest, C., and Foulon, T. (2007) Aminopeptidase B, a glucagon-processing enzyme: site directed mutagenesis of the Zn^{2+}-binding motif and molecular modelling. *BMC Biochem.* **8**, 1−20

91. Pangburn, M.K., Burstein, Y., Morgan, P.H., Walsh, K.A., and Neurath, H. (1973) Affinity chromatography of thermolysin and of neutral proteases from *B. subtilis*. *Biochem. Biophys. Res. Commun.* **54**, 371–379

92. Walsh, K.A., Burstein, Y., and Pangburn, M.K. (1974) Thermolysin and other neutral metalloendopeptidases. *Methods Enzymol.* **34**, 435–440

Acknowledgements

This study was carried out in the Laboratory of Enzyme Chemistry, Division of Food Science and Biotechnology, Graduate School of Agriculture, Kyoto University.

The completion of my doctoral study has been a very challenging and engaging endeavour; one that could not have be achieved without the invaluable assistance of many.

I am heartily thankful to my supervisors, Dr. Kuniyo Inouye, Professor Emeritus of Kyoto University, and Professor Kiyoshi Yasukawa (Ph.D), whose guidance, encouragement, and support from the initial to the final level enabled me to develop an understanding of the subject. Throughout the study, they were patient and provided sound advice, excellent teaching, good company, and a lot of incisive ideas.

I owe a debt of gratitude to Dr. Teisuke Takita, Mr. Kenji Kojima (Assistant Professors, Kyoto University), and a former colleague Dr. Masayuki Kusano all of whose thoughtful discussions and insights broadened my understanding of enzymology.

Further, I offer my regards and blessings to all of those who supported me in any respect during the pursuit of the doctoral course.

I am most grateful to Japan's Ministry of Education, Culture, Sports, Science, and Technology without whose scholarship grant this study would not have been possible.

Last, and most importantly, I wish to thank Mama Yash, Yash, Rhoda, and mum Mrs Emily Menach. To them I dedicate this thesis.

March 2014

Evans P. Menach

List of Publications

Original papers

1. Menach, E., Yasukawa, K., and Inouye, K. (2010) Effects of site-directed mutagenesis of the loop residue of the N-terminal domain of Gly117 of thermolysin on its catalytic activity. *Biosci. Biotechnol. Biochem.* **74**, 2457–2462
2. Menach, E., Yasukawa, K., and Inouye, K. (2012) Effects of site-directed mutagenesis of Asn116 in the β-hairpin of the N-terminal domain of thermolysin on its activity and stability. *J. Biochem.* **152**, 231–239
3. Menach, E., Yasukawa, K., and Inouye, K. (2013) Effects of mutations of thermolysin, Asn116 to Asp and Asp150 to Glu, on salt-induced activation and stabilization. *Biosci. Biotechnol. Biochem.* **77**, 741–746
4. Menach, E., Hashida, Y., Yasukawa, K., and Inouye, K. (2013) Effects of conversion of the zinc-binding motif sequence of thermolysin, HEXXH, to that of dipeptidyl peptidase III, HEXXXH, on the activity and stability of thermolysin. *Biosci. Biotechnol. Biochem.* **77**, 1901–1906